Final Scientific Report
USDOE – DE-OE0000424
University of Arizona Compressed Air Energy Storage

University of Arizona
Tucson, AZ 85721
Joseph H. Simmons and Krishna Muralidharan

Executive Summary of Final Report

Introduction and definition of the research proposed:

Boiled down to its essentials, the grant's purpose was to develop and demonstrate the viability of compressed air energy storage (CAES) for use in renewable energy development. While everyone agrees that energy storage is the key component to enable widespread adoption of renewable energy sources, the development of a viable scalable technology has been missing. The Department of Energy has focused on expanded battery research and improved forecasting, and the utilities have deployed renewable energy resources only to the extent of satisfying Renewable Portfolio Standards. The lack of dispatchability of solar and wind-based electricity generation has drastically increased the cost of operation with these components.

It is now clear that energy storage coupled with accurate solar and wind forecasting make up the only combination that can succeed in dispatchable renewable energy resources. Conventional batteries scale linearly in size, so the price becomes a barrier for large systems. Flow batteries scale sub-linearly and promise to be useful if their performance can be shown to provide sufficient support for solar and wind-base electricity generation resources.

Compressed air energy storage provides the most desirable answer in terms of scalability and performance in all areas except efficiency. With the support of the DOE, Tucson Electric Power and Science Foundation Arizona, the Arizona Research Institute for Solar Energy (AzRISE) at the University of Arizona has had the opportunity to investigate CAES as a potential energy storage resource.

The proposed project divided into several components:

1. Air compression stage – which required the development of a thermal management system to improve operational efficiency and to make available stored heat for injection prior to air expansion.
2. Thermal storage – to allow for retaining the heat of compression and its use prior to the air expansion stage.
3. Storage of compressed air – which required the development of subsurface imaging technology with sufficient resolution and range to determine geological suitability for underground air storage, and the study of the Tucson region to find a suitable geological storage location. (This component was solely funded by SFAZ and is not part of the DOE funded research.)
4. Air expansion engine – to allow for expansion of compressed air to recoup the compression energy efficiently.

5. Economic analysis – to evaluate the cost benefits of the developed technologies.

The research consisted of many phases funded separately by the 3 above-mentioned agencies. The DOE funding was part of the first year of research but was extended at no cost until the end of the 3 years. SFAZ funding was divided into 3 years with equal funding increments. Unfortunately, at the end of year 2, economic conditions at SFAZ caused the end of the support with the exception of a small increment of funds to cover student costs for the 3rd year. The effect of this change drastically affected the completion of this work. Tucson Electric Power funding ws aimed at the demonstration phase of the work and had to be diverted to other purposes when the engine did not function of a sufficient time.

Results from the research:

1. Air Compression stage:

A 3-stage compressor was purchased with air cooling. The cylinders were modified to replace air cooling with water cooling. This removed heat from each compression stage and lowered the temperature of the air passed to the next stage. The advantage of this approach is to increase the efficiency of compression and the overall CAES operation and to send room temperature compressed air into the storage tank. The latter reduces the thermal cycling stresses in the compressed air storage tanks or geological repository. This process adds between 20 and 25% to the efficiency of the compression stage and the overall CAES operation.

Typical CAEs operation has an energy in/out efficiency of about 55%. Just modifying the operation of the compression stage to include liquid intercoolers raises the efficiency to 71% while additionally providing 5% of the input work as stored heat. This offers a potential overall improvement in efficiency of up to 76%.

2. Thermal storage:

Thermal storage studies developed a series of low melting glass compositions to absorb the heat during year 1. Building the high-temperature storage tank was left to year 3. However, the funding cut prevented this portion of the research to be completed. So while we know the compositions of the potential heat storage candidates, we have not optimized the composition for this specific application.

3. Storage of compressed air:

This component of the research consisted of two parts: (a) development of a differential subsurface imaging electromagnetic method and (b) survey of the Tucson Mountains to determine suitability for underground compressed air storage.
The research in this phase was supported solely by SFAZ, and the very successful results are described in their report. For the DOE project, we used a steel 500 gallon 500psi air storage tank.

4. Air expansion engine:

Two types of air expansion or pneumatic engines were tested: (a) turbine type and (b) piston.

For the turbine type, we partnered with a Canadian specialty company that is expert in manufacturing small-scale turbine engines (W-2 Energy). They designed and built several prototypes before concluding that the small air volumes required for economical operation of the small-CAES system were not suitable to turbine engine operation. Typical air leakage from a turbine is too large for the 5 kW systems sought. This approach was abandoned.

For the piston type pneumatic engine, we worked with two undergraduate students in Mechanical Engineering. They designed and built a convergent-divergent nozzle for injection of supersonic air into a cylinder from an air-cooled Volkswagen engine. The nozzle operation was first modeled using finite element analysis and subsequently built. The nozzle performed as modeled and functions perfectly for injecting a small amount of air into the cylinder above a piston. The supersonic speed of the air imparts a large impulse to the surface of the piston which moves it with high torque.

The engine was built to operate with 2 cylinders and the back and forth motion of the driving shaft was transformed to rotary motion using a tri-lobe design. This also functioned properly as designed.

The engine was designed to operate with electrical valves to synchronize the air injection into the cylinders. This did not work as we could not find air valves with sufficient speed at reasonable cost. The electronic valves were replaced by mechanical valves operating from a cam shaft. To date, we have shown that the valves work well, but we are still trying to adjust the timing. In its present form, the engine operates for about 1 or two minutes and the valve timing goes off synchronization. This result shows that the design and much of the operation of the piston CAES expander works, but there remains a valve operation and timing problem which arrests operation after a few engine cycles.

Future applications in the support of power systems for cell towers world-wide look very promising and we are planning to demonstrate the value of adding this small CAES system to the power sources.

5. Economic analysis:

One of the problems of existing CAES systems is lack of efficiency and the large air capacity that they require. Typical CAES efficiencies are 50 to 55%. Minimum CAES turbine sizes are near 100 MW. Smaller applications are not feasible as the turbines cannot be scaled down. Such a large power minimum requires underground air storage in a utility scale application. DOE has spent tens of millions of dollars on two unsuccessful CAES project. The expense is large because of the minimum size requirements.

Failure of the IOWA Storage Initiative was due to poor subsurface imaging techniques which did not reveal the limited permeability of the underground aquifer. The project was abandoned because the stored compressed air could not be withdrawn fast enough to operate the CAES turbines. Failure of the Seneca Lake project resulted when the contractor realized that solution mined salt caves produced by salt companies are not designed to withstand the cyclic pressure changes of a CAES air storage vessel and that new caves had to be mined with specific design for CAES applications.

Our economic study of the small-scale CAES system could not be conducted as the contract was terminated prematurely. We plan to conduct an economic study of the use of 5kW CAES in the support of cell tower operation with future partners.

Project 1 – Compressor efficiency studies
Professor Krishna Muralidharan, students: Vijayanath Veerasamy Kasinathan, Dominique Villela

Introduction / Background

Current commercially available electric-motor driven compressors are major consumers of electric power, and therefore the ability to re-engineer them to significantly increase their efficiencies without compromising their performance is of utmost importance in the context of energy-efficient CAES systems. To achieve this, the fundamental thermodynamics principles characterizing the compression processes need to be examined and identified. Such analysis can then guide the re-designing of available compressors with improved efficiencies. This theory-driven re-engineering of commercial compressors compatible with the requirement of small-scale and medium-scale CAES systems will form the basis of this report. This work provides practical insights into the limitations of commercial compressors and necessary strategies that should be adopted to improve compression efficiency as well as recover compression-heat that would otherwise be wasted. Further, such a study will have a much broader impact given that within the United States, compressor systems account for ten percent of all electricity and roughly sixteen percent of industrial motor system energy use [1]. Further, increasing the efficiency will also have long-term benefits on the longevity of the compressors. Below, is a brief discussion on currently available commercial compressors.

Stock Compressors in Industry

Industrial compressors experience both electrical and mechanical losses often expelleed in the form of heat. As the electric motor does work on the compressor shaft, the mechanics within the motor crank case allow for each piston to compress air to small volumes, increasing the temperature of the volume of air which heats the cylinder side walls and ultimately dissipating this heat through the cylinder heads to the open environment. Most belt-driven devices are air cooled, allowing most of the heat produced to simply blow away as wasted energy. While typical operations blow away heat produced by the compressor motor, there are options for extracting heat from all stages of an industrial compressor, including interstages. This heat can then be stored for use in the compression processes downstream or in compressed-air energy-storage systems, for example, heat can be used in the expansion process to some good work. To make use of that wasted energy by re-introducing it in a manner that can be used, collection and storage of any lost heat is critical.

In general, increased compression-efficiency can be enabled via the following methods:

1. Proper and Efficient Compressor Selection for the Application
2. Compressor Metering and Control for Cyclic Demand
3. Demand Control and Optimization
4. Reduction in System Pressure
5. Efficient Cooling System Design
6. Heat Recovery and Reclaim
7. Elimination of Inappropriate Uses
8. Improving Maintenance

Out of the above eight methods, the most relevant are (5) and (6), which form the bulk of compression-operation costs (~ 73 % as identified in Fig. 1). Strategies to improve (5) and (6) will be followed in this work.

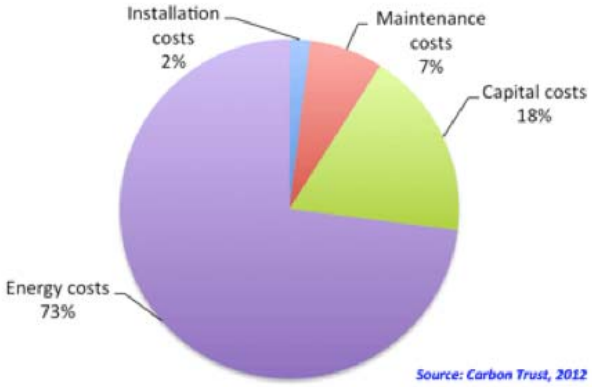

Figure 1: Cost associated with a commercial compressor

Two classes of commercial compressors are available: positive-displacement and dynamic. An example of a positive-displacement class includes a bicycle pump, which changes the volume of a chamber to compress air. When a piston inside a cylinder forms the compression chamber, the compressor is said to be reciprocating. Out of reciprocating compressor machinery, there are both single-acting and double-acting pistons which range from fractional horsepower to over 600hp (3).

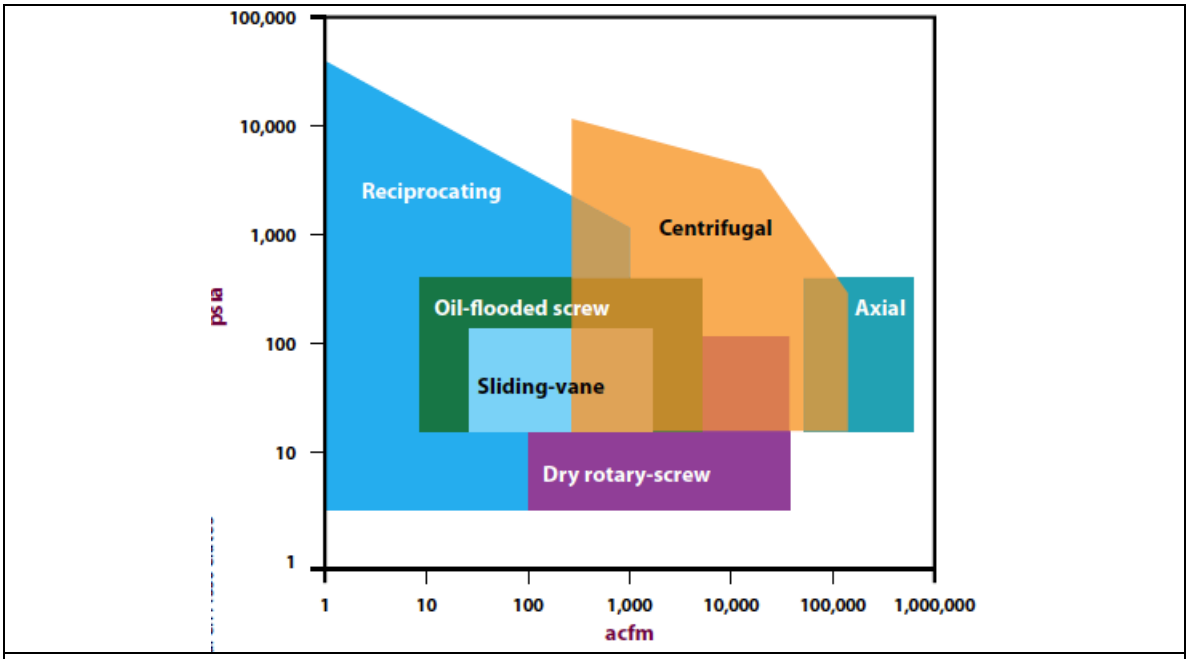

Figure 2: Typical operating regimes for different compressor types [2]

Positive-displacement reciprocating compressors can be single-stage or multi-stage. While there are other compressor types such as screw, rotary vane, centrifugal, and axial, the reciprocating compressor are more compatible with the needs of this work- i.e. access to modify

interstage processes. Intercoolers between each stage of compression allow the output of one cylinder to be cooled before being compressed in the next cylinder stage, ultimately cooling the in-line air for efficient compression. Further, output pressures from positive-displacement systems produce the greatest pressure, especially when a multi-stage compressor is used. In this work, we use a 3-stage reciprocating positive-displacement compressor: the 3-Stage Bauer Vertecon Medium Pressure Industrial Air Compressor Unit (VIB 12.4 II), manufactured in Germany.

Thermodynamics of Compression

Isothermal and Adiabatic Processes

For reciprocating compressors, thermodynamic models can be used to provide useful guidelines to characterize the compression process and therefore quantify the extent of deviation of the actual compression process from thermodynamics predictions. The compression process is bounded by two limits, namely the isothermal and adiabatic limits, with the polytropic index of these compression processes equaling 1.0 and 1.4 respectively. Here, the polytropic index corresponds to the path that relates the initial and final states of compression. Typically, the polytropic of a 'real' compression process falls between 1 and 1.4. Fig. 3 depicts the pressure(P)-volume (V) characteristics of the different compression processes. The associated work done is related to the area and under the respective curves, and it is evident that the work done in the isothermal process is the least and is maximum for the adiabatic case. The isothermal process is accompanied by no temperature change in the compressed-gas/air, in contrast to the large temperature increases characteristic of adiabatic compression.

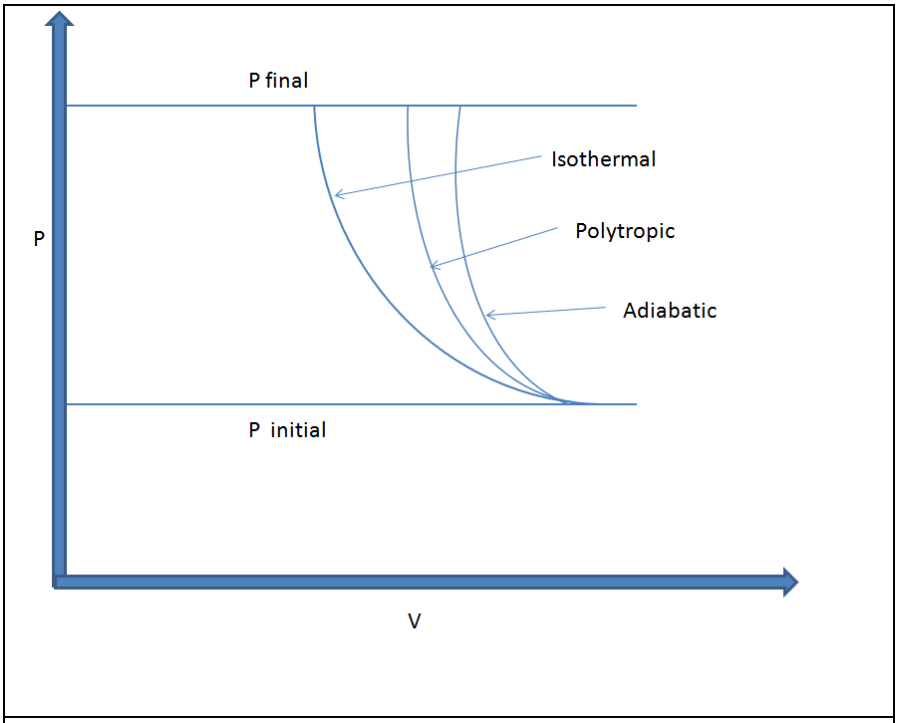

Figure 3: PV Diagram for Various Polytropic Compression Processes

Single-stage and Multi-stage Compression

Commercial high-pressure compressors usually employ multi-stage compression processes, in order to improve efficiency of compression such as the selected compressor in our work. Multi-stage compressors have in-built intercoolers between the different stages to aid the extraction of heat of compression to surroundings, to bring the process closer to isothermal conditions. This is shown in Figure 4, where the highlighted area represents the energy saved by removing heat at the intercoolers. Nevertheless, it has to be pointed out that these commercial compressors use external cooling air-fans to remove heat of compression at the intercoolers, which is not the most efficient method of heat removal.

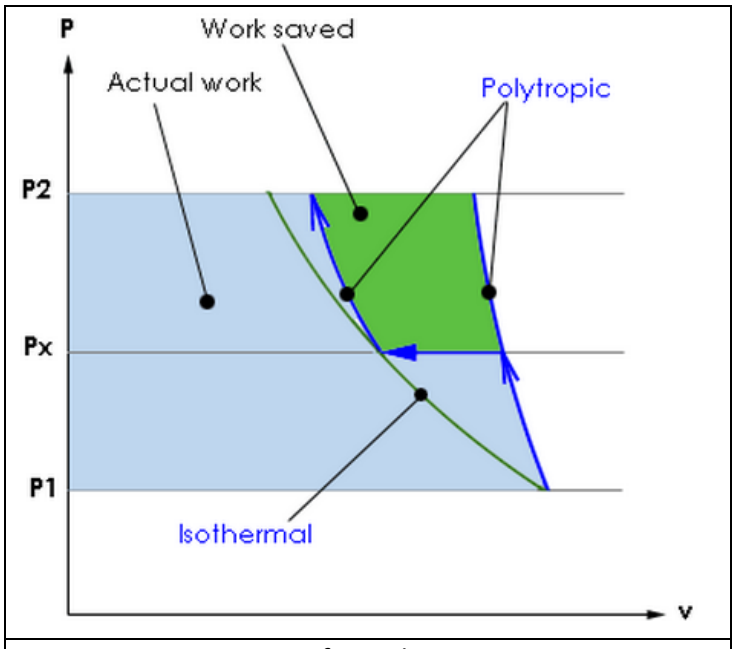

Figure 4: PV curves for multistage compression

Mechanics of a 3-Stage Compressor

For small-scale to medium-scale CAES, an optimal maximum pressure of storage is between 500-1000 psig. In order to ensure reasonable efficiency of the compression process, appropriate intermediate pressures have to be specified to ensure compression efficiency. The following discussion will shed light on the choice of the intermediate values of pressure.

Assuming that

1. Compression process in isentropic with no pressure drop in the intercoolers
2. Inlet temperature to all stages is the same
3. Specific heat (C_p) and specific heat ratio (n) are constant

The compressor work input per unit mass flow is:

$$\frac{W}{\dot{m}} = \left(h_{stage1} - h_{initial}\right) + \left(h_{stage2} - h_{stage1}\right) + \left(h_{final} - h_{stage2}\right)$$

$$\frac{W}{\dot{m}} = c_p\left(T_{stage1} - T_{initial}\right) + \left(T_{stage2} - T_{stage1}\right) + \left(T_{final} - T_{stage2}\right)$$

From the assumption that all intermediate stage inlet temperature is $T_{initial}$,

$$\frac{W}{\dot{m}} = c_p\left(T_{stage1} - T_{initial}\right) + \left(T_{stage2} - T_{initial}\right) + \left(T_{final} - T_{initial}\right)$$

$$\frac{W}{\dot{m}} = c_p T_{initial}\left\{\frac{T_{stage1}}{T_{initial}} + \frac{T_{stage2}}{T_{initial}} + \frac{T_{final}}{T_{initial}} - 3\right\}$$

Expressing the temperature ratios as pressure ratios:

$$\frac{W}{\dot{m}} = c_p T_{initial}\left\{\left(\frac{P_{stage1}}{P_{initial}}\right)^{\frac{n-1}{n}} + \left(\frac{P_{stage2}}{P_{stage1}}\right)^{\frac{n-1}{n}} + \left(\frac{P_{final}}{P_{stage2}}\right)^{\frac{n-1}{n}} - 3\right\}$$

For a specified value of $T_{initial}$, c_p, $p_{initial}$ and p_{final} the compressor work input varies with intercooler pressure. Minimizing with respect to the inter mediate pressures, and simplifying:

$$Pint1 = \sqrt{Patm * Pint} \qquad Pint2 = \sqrt{Pint1 * Pfinal}$$

For example, solving for the optimal intermediate pressure for a 3-stage compressor operating from 14.7 to 1000 psig, Pint1 = 60.03 psi and Pint2= 244.95 psi. Next, we will evaluate the work done for different compression scenarios.

<u>Thermodynamic work Input for a 3-stage compression process</u>

A thermodynamic model for work input (W) to the compressor per unit mass (m) of air for various polytropic processes is calculated as given below:

$$\frac{W}{\dot{m}} = RT\ln\left(\frac{P_{final}}{P_{initial}}\right) \text{ .... (1)}$$

Here n is the polytropic index, R is the Avogadro gas constant and T_2 and T_1 represent the final and initial temperatures (i.e. after and before compression). Note that when n=1, then

$$\frac{W}{\dot{m}} = \frac{nR}{n-1}\left(T_2 - T_1\right) \text{ .... (2)}$$

The temperature at the end of each stage can be calculated by knowing the ambient temperature and final pressure,

$$T_2 = T_1\left(\frac{P_{final}}{P_{initial}}\right)^{\frac{n-1}{n}} \quad \ldots\ldots (3)$$

The following table lists the total work input needed for compressing air from 14.7 psi to 1000 psi into a 500 gallon tank, as a function of polytropic index. Clearly, the closer the compression process is to the isothermal case, the less the work consumed (and higher the efficiency).

Table 1. Total Work to Compress Air from 14.7 psi to 1000 psi into a 500 gal. Tank as a Function of Polytropic Index	
n	Work input (MJ)
1	55.3
1.1	66.9
1.2	80.29
1.3	93.62
1.4	107.415

Exergy Analysis of Compressed-Air Storage Process

The useful energy that can be extracted from the stored compressed air is defined as exergy. The useful energy is calculated by finding the difference in the energy between the stored compressed air and the ambient conditions. This gives the limit to the maximum possible useful work that can be extracted from the tank. Exergy per unit mass (e) is calculated from the knowledge of initial and final pressure, volume and entropy content respectively, as given below:

$$e = (u - u_0) + P_0(v - v_0) - T_0(s - s_0) \quad \ldots\ldots (4)$$

The exergy of compressed air stored at 1000 psi in a scuba tank (0.5 gallon) and in a 500 gallon tank is calculated as a function of polytropic index and tabulated below and as expected, isothermal conditions ensure maximum exergy.

Table 2. Total Exergy of Stored Compressed-Air		
n	Scuba tank (80 cubic ft.) (kJ)	500 gallon tank (MJ)
1	31.1	42.15
1.1	20.06	27.05
1.2	15.7	21.4
1.3	14.7	19.9
1.4	13.1	20.1

Having discussed the fundamental thermodynamic principles that govern compression processes, we now turn our attention to a commercial compressor, namely a three-stage compressor built by Bauer, which suits the needs of our project.

3-Stage Bauer Compressor Characterization

Specifications Overview

The Bauer Vertecon Medium Pressure Industrial Air Compressor Unit (VIB 12.4 II) is a 5 hp reciprocating unit operating at 1200 rpm and has a maximum pressure of 1000 psig, charging at a rate of 8.0 cfm (See Table X below for a specifications listing).

The Bauer compressor is belt-driven, driving a pulley that also doubles as a primary fan and rotates the main crankshaft. This primary fan in turn blows air across the compressor fins to cool during the compression process. The 3-stage Bauer is equipped also with 2 intercoolers, one between stages 1-2 and another between stages 2-3.

Given that this compressor relies on forced-air cooling at the intercoolers, a significant improvement in the performance of the compressor can be obtained, by switching to a much more efficient liquid-cooling system to assist in the removal and storage of wasted heat of compression. The development of such a liquid-cooler will ensure the increase in compression efficiency as well as provide a path to store the excess heat produced and re0use it during the extraction phase.

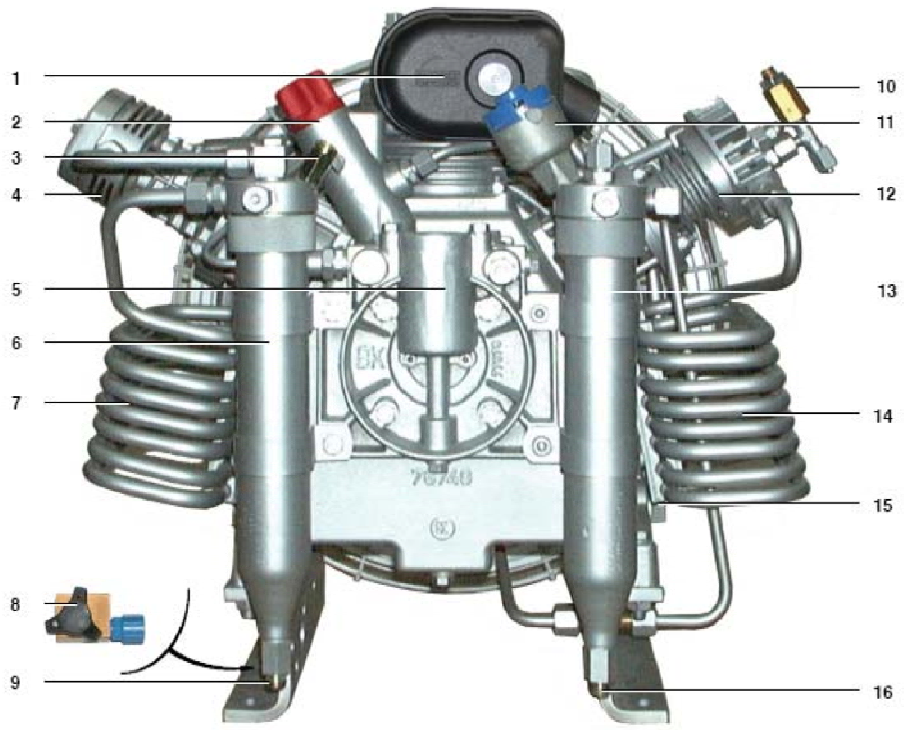

Figure 5. Stock Compressor Cooling System. 1) Intercooler 1st to 2nd stage, 2) Intercooler 2nd to 3rd stage.

Re-Engineering the Bauer Compressor for Heat Extraction

Experimental Setup

A 3-stage Bauer Vertecon Medium Pressure Industrial Air Compressor Unit (VIB 12.4 II) was customized to extend and distance stock intercoolers away from the body of the compressor crankcase (casing) using high-pressure lines. Fittings were modified on the German designed compressor, and flexible high-pressure lines were selected and connected. The select high-pressure hydraulic lines are Titeflex Type R115, with an operating pressure of 1500psi, well above the 1000psi rating of the commercial 3-stage compressor. R115 hoses are lined with non-conductive PTFE (Dupont type 62 fine grade resin) and have an braided 304 stainless steel exterior reinforcement. R115 has an operating temperature of -65F to +400F (-54C to +204C) for continuous service or -100F to +500F (-73C to +260C) for intermittent service.

Two open-system (open-air) water baths were built using stainless steel containers and at the appropriate height for the industrial compressor crankcase body. A total of two 16-Liter water tanks were modified to have inlets and outlets for water lines. Barbed fixtures were welded to the side of the tank bases and red RTV sensor-safe / high-temperature silicone was added as a gasket at all weld points (inlets and outlets) to primarily prevent corrosion. A curing period of 24-hours followed for the RTV product to form a red tough, flexible, silicone rubber gasket. The resultant silicone rubber gaskets are said to resist temperatures of up to 600F (316C).

Stainless steel stands (frames) were fabricated and both water baths were spot-welded to these supporting stands. The water baths were physically distanced from the compressor crankcase to disperse high-heat sources away from the central mechanical compressor system.

The pair of modified intercoolers was then submerged in the custom water baths for liquid cooling. Water containers were kept open to allow heat to escape by thermal convection. High-temperature clear polyvinyl tubing was attached to the barbed fixtures to allow circulation of water between each water container. Maximum operating temperatures of 175F (79C) are allowed for the PVC tubes. Lines crossed over the steel framing of the 3-stage compressor, but did not touch the crankcase.

Between the water baths, a standard automotive air-cooled transmission radiator was installed per the manufacturer recommendations for “in-series” cooling. The radiator comes from the manufacturer with electrostatic powder coating to resist corrosion. Two submersible (underwater) pumps were installed on the inside of each water container, pulling liquid into the pump from a bottom-intake and circulating water at approximately 80gph through the “in-series” cooling radiators. Wet-rotor pump types were selected for energy efficiency (5.5 watts) during continuous operation.

Given below is a summary of all modifications made to the intercoolers to incorporate liquid-cooling within the compressor and Fig. 6 illustrates the modified compressor.

Table 3. Materials	
Application	Description
Intercooler Line Extensions	Titeflex Type R115 2250psi, 1500psi and under is operating pressure, Titeflex R115 PTFE hose contains innercore which has been extruded vertically to maintain the highest quality of concentricity. Titeflex PTFE is manufactured from Dupont type 62 fine grade resin or equivalent and uses 304 stainless steel wire braid as reinforcement. Titeflex R115 hose innercore is non-conductive PTFE with a wall thickness of 0.030". Titeflex R115 Series hose sizes -4 through -10 are rated for full vacuum. Larger sizes -12 and above can be reinforced with an internal support spring for full vacuum service. Titeflex R115 Series hose has an operating temperature range of -65°F to +400°F (-54°C to +204°C) for continuous service or -100°F to +500°F (-73°C to +260°C) for intermittent service.
Water Baths	Stainless steel water baths holding 16L each. Water baths were welded onto custom frames for stabilization and height purposes.
Water Lines	Watts (A Water Technology Company) Clear Polyvinyl tubing. Lead free PVC with the clarity of glass. Smooth dense bore maximizes flow and reduces sediment buildup. Resistant to acids, alkalis, and a variety of chemicals, gases, and liquids.
Custom Intercoolers	Stock Bauer Intercoolers Modified to Custom Fittings 1st Stage intercooler (Part # 081309) and 2nd Stage Intercooler (Part # 078195)
Water Pumps	Crystal Pond Professional Foundatin Pump Model DP80A (A total of two were used) - Energy efficient 5.5 watts - 80gph @1' lift
Transmission Cooler / Radiator	Hayden Automotive Rapid Cool Trans-Cooler Specifications: - OEM type plate and fin design - Space efficient design fits more vehicles - Electrostatic powder coating to resist corrosion
Coolant Additive	Red Line Synthetic Oil: Water Wetter Super Coolant - Unique agent for cooling systems that doubles the wetting ability of water - Rust and corrosion protection allows for use of straight water in racing or reduced antifreeze levels in warm climates - Improves heat transfer and reduces cylinder head

	temperature

Comparison of Stock and Modified Compressor

Liquid vs. Air Cooling

Modified Compressor Efficiency Results and Considerations
Air Cooling vs. Liquid Cooling at Intercoolers

Liquid Recirculation
Effective removal of the heat from the air passing through the intercooler coils is achieved by the liquid bath. The liquid bath removes the heat and keeps the air passing to the next stage at ambient temperature. The heat is absorbed by the liquid and the temperature of the bath increases. The water in the liquid bath is circulated through a radiator, in which the water is cooled and is returned to the bath at ambient temperature. The circulation of water keeps the water at ambient temperature. As long as the water in liquid bath stays at ambient temperature, the air passing through the intercoolers and reaching the inlet of the next stage will be at ambient temperature. The circulation of water from the bath to the radiator is a way to effectively increase the heat dissipation to the surroundings.

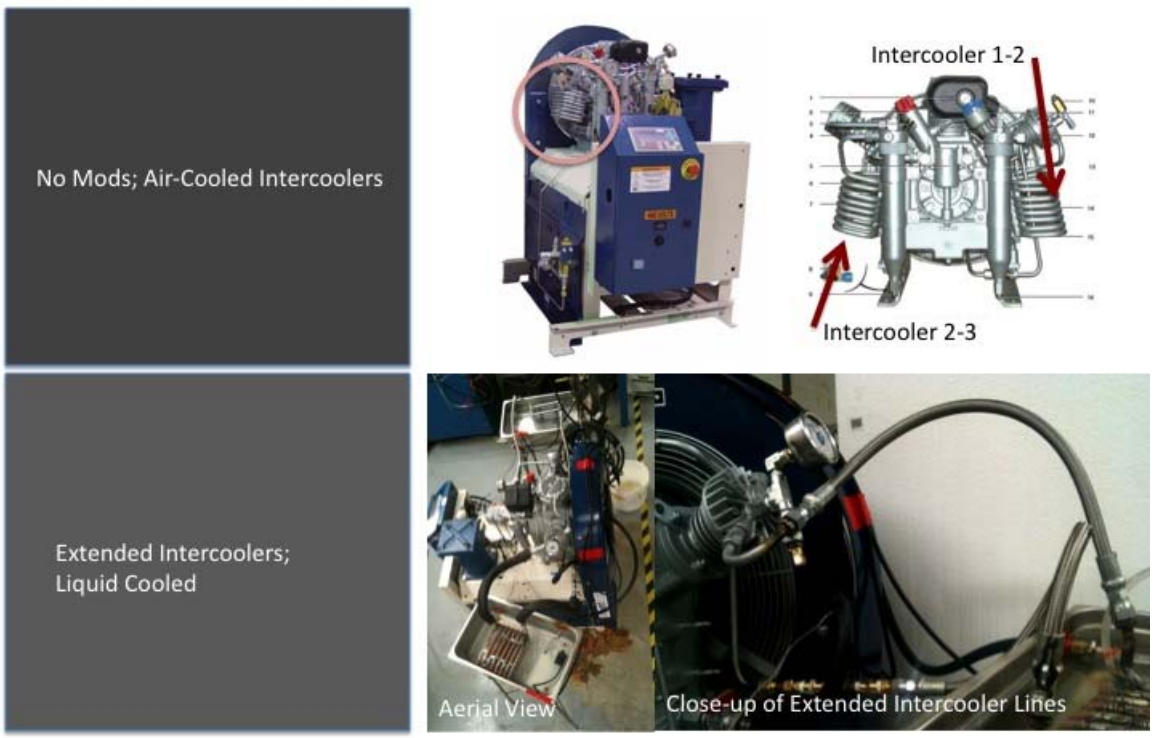

Figure 6: Stock Vs modified intercoolers

Temperature Control with Liquid Bath

The experimental measurements of the temperature at the intercoolers are shown in graph. These measurements were taken between stages 1 and 2 as well as 2 and 3. T1 is the outlet temperature after stage 1, which feeds through the high-pressure intercooler line and back into stage 2, where T2 is the temperature of the air after being cooled. T3 is the outlet temperature after stage 2, which feeds through the high-pressure intercooler line and back into stage 3, where T4 is the temperature of the air after being cooled. Liquid cooling at the intercoolers brings the air temperature to ambient temperature by more effectively removing the compression-heat. This is evident from the temperature data at the inlet and outlet of the intercoolers as given in Figs. 7 and 8, which illustrate the temperature variation of the liquid bath for the stock vs liquid-cooled systems. The pressure drop through the modified intercooler length is the same for both modified and stock compressors. The gain in overall efficiency due to liquid cooling is reflected in (i) reduction in work done and (ii) amount of thermal-energy extracted. This data is tabulated in Tables 4 and 5, which represent two operating conditions-(filling up a scuba tank and a 500-gallon tank at 500 psi, which are shown in Fig.9)

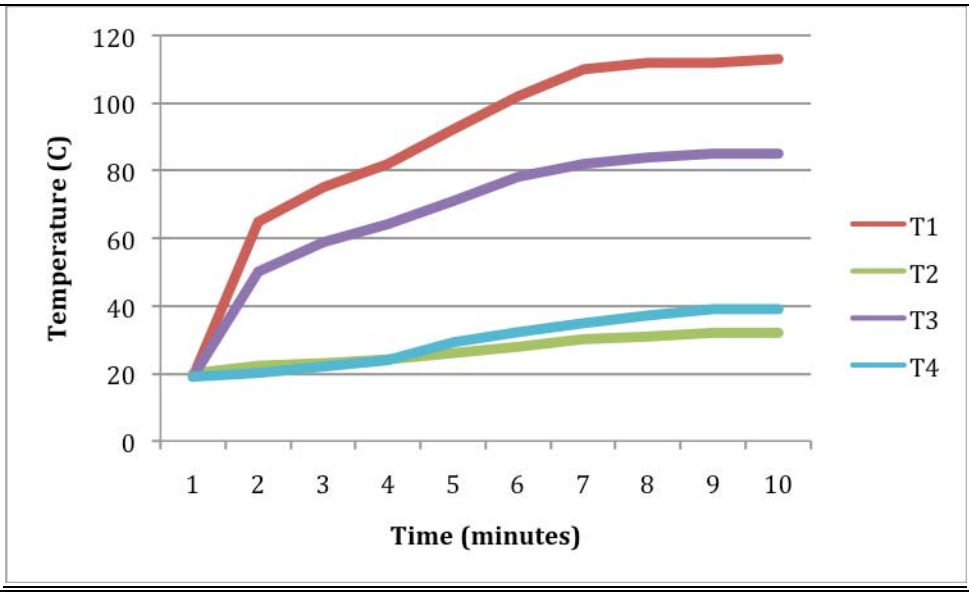

Figure 7: Stock Air-Cooled Intercooler Temperature Before and After Intercooler (T1 and T2 are for Stage 1-2; T3 and T4 are for Stage 2-3); Compression into Scuba Tank from 0-1000psig

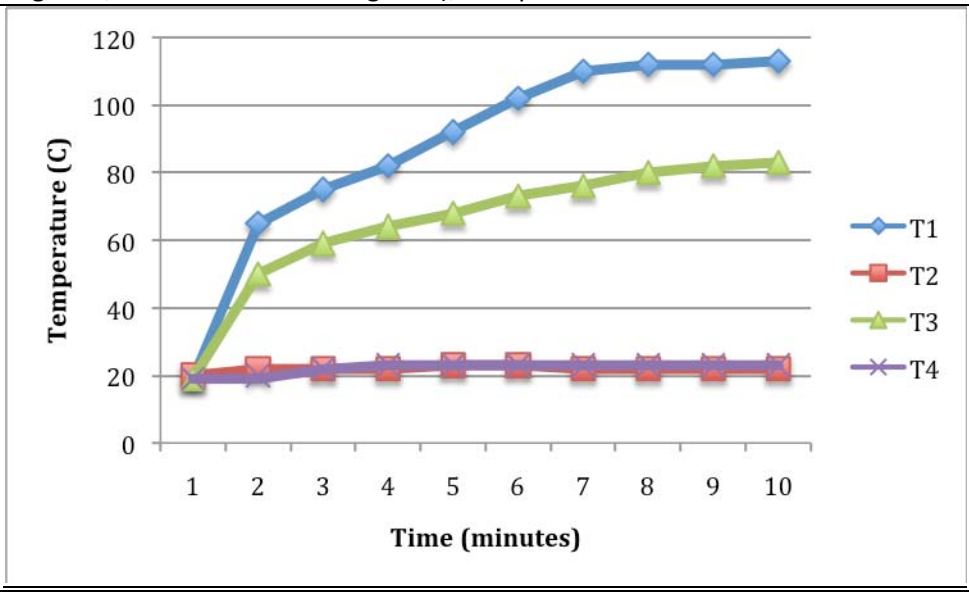

Figure 8. Modified Extended Liquid-Cooled Intercoolers (T1 and T2 are for Stage 1-2; T3 and T4 are for Stage 2-3); Compression into Scuba Tank from 0-1000psig

Figure 9: A 500 gallon tank and a scuba tank

500 gallon tank	
time of operation	360 (min)
Power consumption	
with stock cooling	with liquid cooling
356 MJ	300 MJ
power reduction	16%
Heat extracted	12 MJ
Increase in efficiency	20%

Scuba Tank	
time of operation	10 (min)
Power consumption	
with stock cooling	with liquid cooling
160 kJ	140 kJ
power reduction	12%
Heat extracted	20kJ
Increase in efficiency	25%

In conclusion, based on sound theory-based recommendations, appropriate modifications were made to the intercoolers of a commercial compressor. Specifically, using a novel liquid-cooling based heat-exchanger, the efficiency of the compressor-operation was shown to increase by at least 20 %. Equally importantly, via the liquid-cooling system, heat of compression was extracted, which can then be used during the energy extraction process. This has profound implications in the design, development and deployment of energy-efficient CAEs systems.

APPENDIX 1.

Symbols:

Lower case alphabets represent entities on unit mass basis

e-specific exergy

u-specific internal energy

v-specific volume

s-specific entropy

h- specific enthalpy

T-temperature

R -gas constant for air

n-specific heat ratio

c_p -specific heat at constant pressure

Subscript

o – ambient state

initial – initial stage/ambient conditions

final – final stage 1000psi

stage1,2,3 – intermediate stage 1,2,3

Project 2 - Glass Materials for Application as Novel Heat Transfer and Storage Fluids in Solar Energy Collectors and Energy Storage

Erica L. Corral

Materials Science and Engineering Department
Arizona Materials Laboratory

College of Engineering
The University of Arizona
Tucson, AZ

February 15, 2010

Research funding provided by
Science Foundation Arizona-Solar Technology Institute.

Students supported on this project V. Marotto, and J. Zwick

Advanced thermal storage fluids are needed in order increase heat-to-electric efficiencies of solar powered technological devices

- A variety of molten salts and liquid-fluoride-salt are used as heat transfer fluids in solar towers.
- During the daytime the liquid salts deliver heat at temperatures between 300 and 850 °C but at night time there is a need for fluids that store energy at lower temperatures (< 100 °C) in order to operate at nighttime.
- New materials are needed that operate at temperatures less than **200 °C**, while maintaining a high capacity for thermal storage in day and nighttime environments.

Molten Salt Solar Receiver

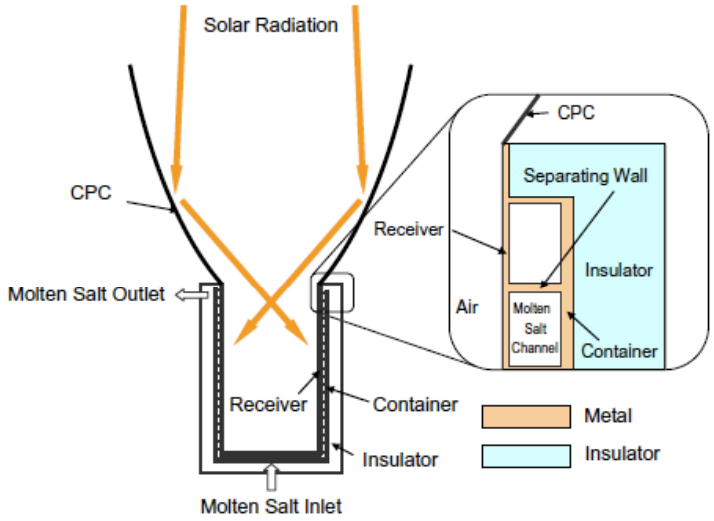

H. Hasuike, Y. Yoshizawa, A. Suzuki, Y. Tamaura, "*Study on design of molten salt solar receivers for beam-down solar concentrator*," Solar Energy **80** pgs. 1255-1262 (2006).

CAES Application

- CAES stores energy by a compression stage
  - Air compression creates heating
- CAES releases energy by an expansion stage
  - Air expansion creates cooling
- With no thermal recovery, the in-out efficiency is below 65%
- With thermal recovery and heat transfer from the compression to the expansion stage, the in-out efficiency can go up to 85%.
- But heat transfer requires intermediate energy storage and low temperature storage materials.

Molten salt mixtures are being investigated for possible use at low temperature thermal storage fluids

Molten Salt Mixture*	Specific heat (kJ/ kg K)	Viscosity (mm^2/s)	Thermal Conductivity (W/m K)	Melting Temperature	Max Temperature
$NaNO_3$/ KNO_3	1.46	0.855	0.4215	220 °C	600 °C

*Salt mixture is 50/50 wt% and is currently used as a heat-transport fluid in non solar applications.

However these materials crystallize into dense material at temperature less than 300 °C and we are developing glass materials as novel low temperature storage fluids that do not crystallize at temperatures less than 80 °C.

Fluoride based glasses posses most of the requirements for low temperature thermal storage fluids

Fluoride based glasses possess:

- Low glass transition temperature, Tg < 70 °C
- High heat capacity,
- Low viscosity at temperatures less than 100 °C
- But have yet to be studied for this application

Good Glass Formation Region for Lead fluourosilicate glasses

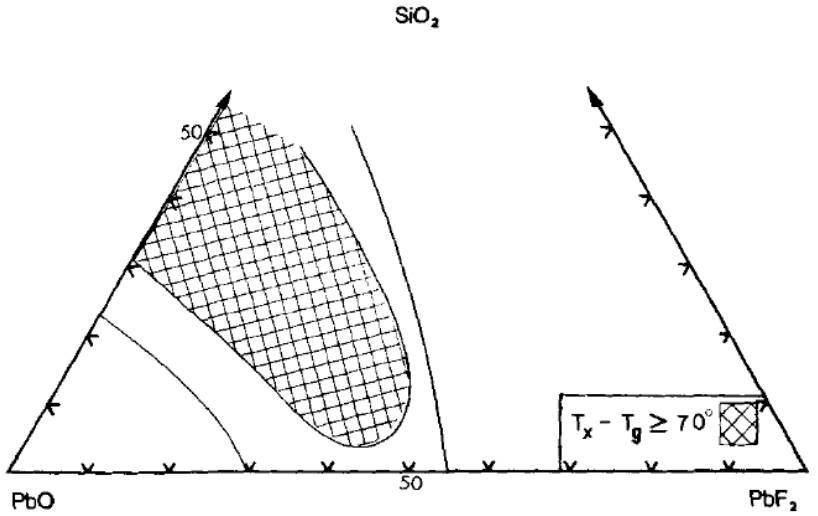

J. Coon and J. E. Shelby, "Properties and Structures of Lead Fluorosilicate Glasses," J. Am. Ceram. Soc. **71** pgs. 354-357 (1998).

Our approach is to develop low T_g lead fluorosilicate and phosphate based glasses for use as novel low temperature thermal storage fluids.

Various glass compositions were processed in order to investigate glass transition temperatures

Glass Processing & Characterization Method

Glass Compositions (mol %)

Glass Number	Tg (°C)	PF_6	PO_4	SnF_2	SnO	PbF_2	ZrF_4
1	**85**		17.4	56.4	14.1	12.1	
2	**85**		17.4	55.4	17.3	9.9	
3	**164**	10.2	19.0	70.8			
4	**164**	9.3	27	62		1.7	
5	**77**		2.3	96.2	1.3	0.2	
6	**88**		28.3	47.2	12.5		12.0
7	**97**		25.5	50.5	15.1		8.9

Differential scanning calorimetry (DSC) measurements were used to characterize glass transition temperature

Typical features of a DSC curve

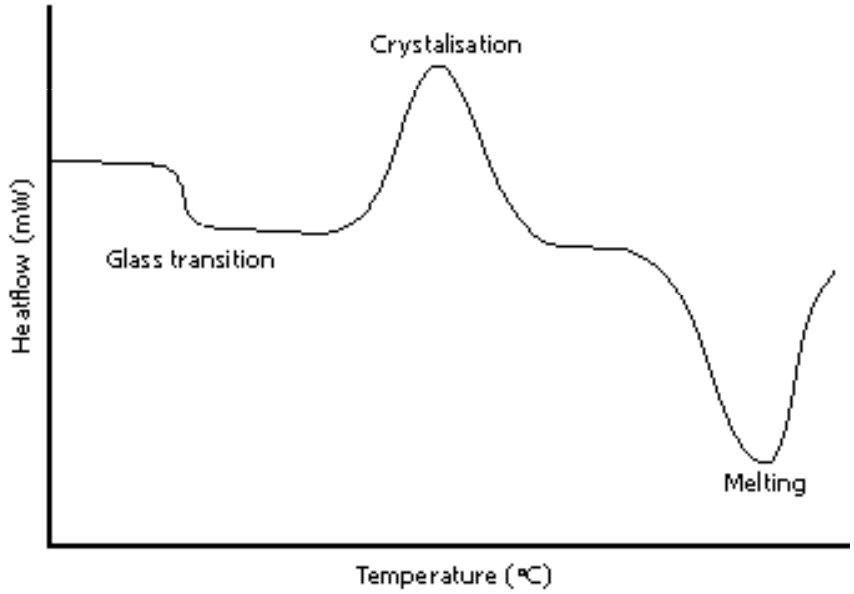

- DSC was used to investigate the effect of glass composition and processing methods on glass transition temperatures.
- DSC curves are used to also identify crystallization and melting temperature of the glass compositions.
- A heating rate of 15 °C/min promoted the formation of distinct glass transition peaks.
- Temperature range tested from room temperature to 300 °C.

Characterization of glass behavior with increasing temperature is necessary in order to use the materials as reliable storage fluids.

Lead-fluorosilicate glasses, rich in Sn concentrations, exhibit glass transition temperatures from 77-85 °C

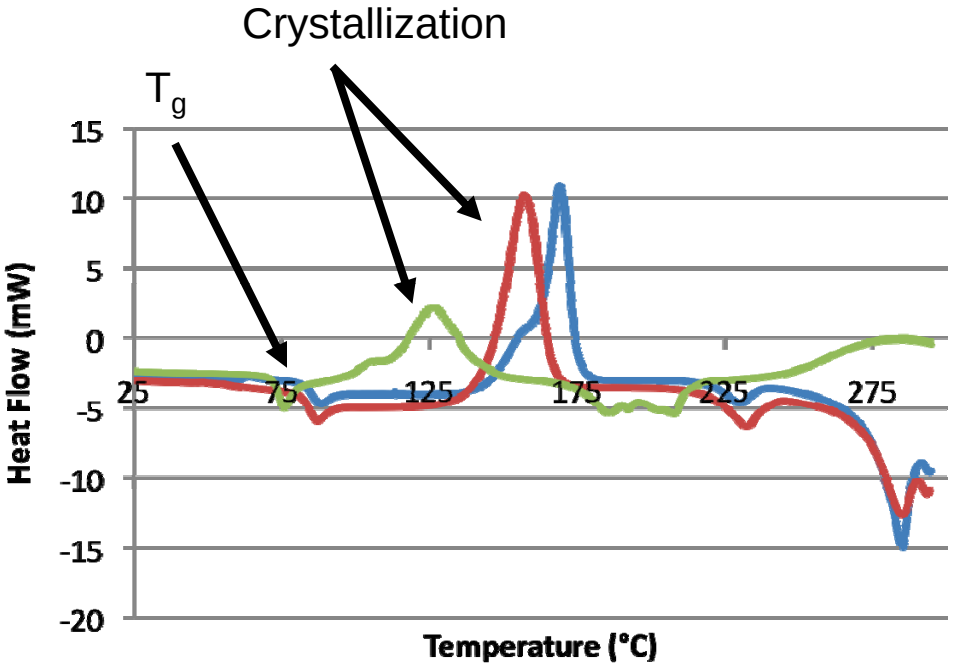

Number	Tg (°C)	PO_4	SnF_2	SnO	PbF_2
1	**85**	17.4	56.4	14.1	12.1
2	**85**	17.4	55.4	17.3	9.9
5	**77**	2.3	96.2	1.3	0.2

- **Crystallization temperature decreases with decreasing Pb concentration.**
- **Glass transition temperatures are the same for similar glass compositions, G1 and G2, which are rich in Sn concentration.**
- **Overall, melting and mixing processes during melting were reproducibly and produced transparent glass materials.**

ArizonaMaterialsLaboratory

Tin fluorosilicate glass exhibit glass transition temperatures around 164 °C with and without Pb additions

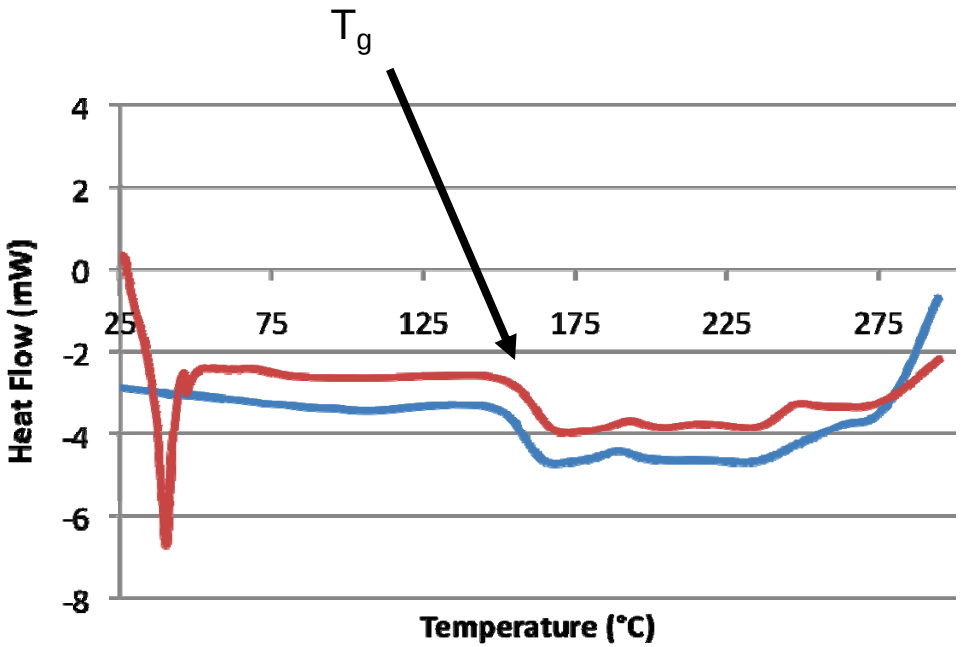

Glass Number	Tg (°C)	PF_6	PO_4	SnF_2	PbF_2
3	**164**	10.2	19.0	70.8	
4	**164**	9.3	27	62	1.7

- Crystallization and glass transition temperature are well above 150 °C.
- Glass transition temperatures are considerably high for Sn rich compositions.
- Overall, melting and mixing processes was not very uniform and re-melting the batch at temperatures greater than 430 °C is necessary.

Tin fluorosilicate glass exhibit glass transition temperatures between 88-97 °C with Zr additions

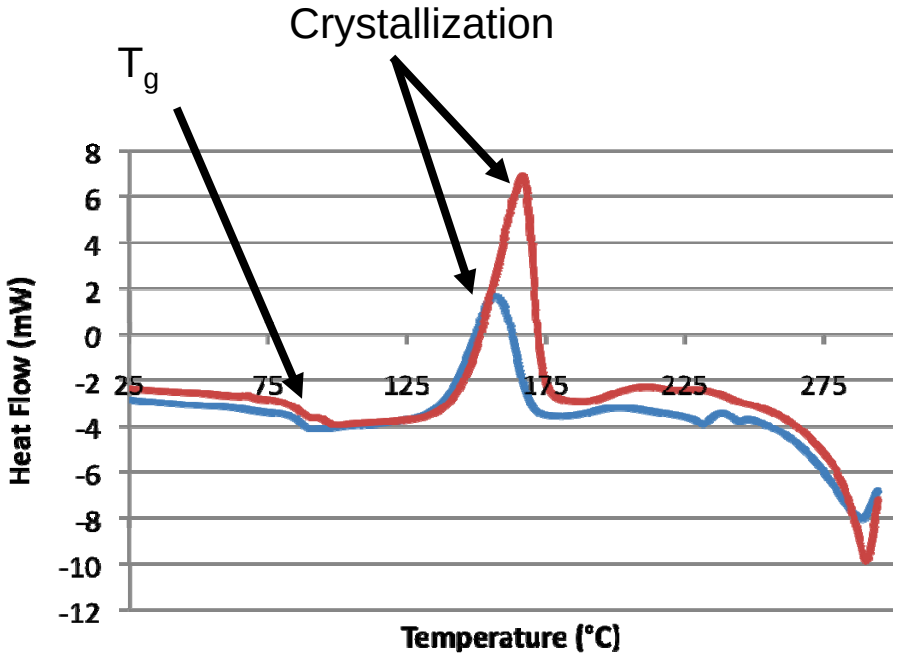

Glass Number	Tg (°C)	PO_4	SnF_2	SnO	ZrF_4
6	**88**	28.3	47.2	12.5	12.0
7	**97**	25.5	50.5	15.1	8.9

- **Crystallization temperatures are between 160-170 °C for Zr containing glasses.**
- **Glass transition temperatures are between 88-97 °C for similar glass compositions, G6 and G7.**
- **During melting their was some residual impurities that could have effected thermal properties of the glasses.**
- **We are investigating new melting procedures and methods for batch mixing in order to enhance homogeneity of the melt.**

ArizonaMaterialsLaboratory

Summary

• A suite of lead and lead free fluorisilicate glasses were processed in order to characterize the low glass transition temperatures for potential use as low temperature thermal storage fluids.

• The lowest glass transition temperatures measured were between 77-88 °C for glass compositions with high lead and tin concentrations (G1, G2 and G5).

• However, it was difficult to homogeneously melt the glass compositions due to volatility of the glass constituents. Therefore, a series of high temperature melt temperatures (450, 500, 550, and 600 °C) are underway in order to characterize the effect of melt temperature on thermal properties and homogeneity of the melt.

• In addition, cyclic thermal analysis measurements are underway from room temperature up to 300 °C in order to investigate the effect of glass crystallization on glass transition temperatures.

Project 4 - Pneumatic CAES Engine – Krishna Muralaidharan, Joseph Simmons, students: Matthew Jordan, Sean Athanasios Katsarellis

This engine is capable of running on compressed air alone, or compressed air in conjunction with a combustion system. The working fluid may be simply compressed air, heated compressed air, or the combustion products of compressed air and a fuel. The working fluid is induced through a converging-diverging nozzle into a piston chamber. The pressure of the working fluid forces the piston to displace, until the working fluid is exhausted out of the piston chamber. As the piston is moved, it contacts a special type of camshaft, called a trilobe shaft. This contact applies to torque to the trilobe shaft, causing it to spin. This rotational motion is used to turn an electrical generator to produce electricity.

The trilobe shaft assembly consists of the main shaft, two trilobes (a triangular shaped piece with rounded lobes instead of corners), and a spacer to separate the two trilobes. Each cylinder assembly is made of a piston, cylinder sleeve, and a cylinder head. Each cylinder head has a converging-diverging nozzle placed inside of an external casing. The connecting rod assembly is the actual connecting rod along with cam wheels supported by dowels. The casing may have any form or material, so as long as it properly supports all the required components for operation. This arrangement is for two rows of horizontally opposed cylinders, but the shaft may be longer or shorter to accommodate more or less cylinders. Shaft dimensions and geometry may vary as well, so long as the trilobes are designed properly.

This arrangement has two parts: the cylinder block and the cylinder head. The cylinder block is simply a tube made to accommodate a sliding piston and varying pressures. The cylinder block will also have exhaust holes drilled circumferentially around it. The distance from the top of the cylinder block to these exhaust holes is the desired displacement of the cylinder. The geometry of the cylinder may vary so long as it accomplishes the previously stated purposes. The cylinder head is made of a casing enclosing a converging-diverging nozzle. This converging-diverging nozzle (CDN) may be machined into the casing or into another piece of metal. The casing is meant more for protection and structural support whereas the CDN is to be designed for desired flow characteristics.

The primary function of the converging diverging nozzle is to efficiently use compressed stored air and provide a great amount of force on the piston heads of the engine. The selection of the converging diverging nozzle was based on how it efficiently accelerates the compressed air to higher speeds. The benefit of using the converging diverging nozzle configuration in the relation to compressed stored air is that it takes advantage of the high pressures that the air is stored and thus reaches supersonic velocities. Because of the flow acceleration, the force that is exerted at the nozzle exhaust achieves a great amount of thrust that can be efficiently used towards the engine operation. This is superior when compared to other ways that are used to create a force on the piston head, as it uses the same amount of mass flow but at the same time it creates a higher amount of force at the exit. The reason for providing a better performance is

because of its converging diverging shape. The shape is the primary reason for accelerating the flow from the given subsonic flow speed, at which the compressed stored air is released at, to higher subsonic or in most cases supersonic speeds. As mentioned earlier, this results in creating a higher amount of force towards the end of the nozzle.

The nozzle is designed to reach supersonic speeds, but this might not be the optimum as far as the engine operation is concerned. The reason is that when the flow reaches supersonic speeds, shockwaves are generated, which can sometimes lead to significant pressure drop that will slightly decrease the amount of thrust that is being reached at the nozzle exhaust. However, the decrease in thrust is not significant and even this decreased amount of thrust is superior to the amount of thrust that other cylinder head configurations can produce. The nozzle is basically designed so that even when the flow reaches higher subsonic speeds the generation of force provided at the exit is still greater than a simple cylinder head design. Therefore, whichever case is considered, flow reaching supersonic or subsonic speeds, the thrust achieved at the exit of the nozzle is far superior to other ways of generating a force on the piston head, while using only compressed stored air as the propellant.

As mentioned earlier the profile shape of the pneumatic accelerator has a converging diverging shape. The profile of the nozzle plays a great role in the overall performance of the pneumatic accelerator. By optimizing the profile shape it has been proven that the performance can be increased and thus increase the amount of force generated on the piston head. The method used to create a smooth converging diverging profile is called Method of Characteristics. This method is simply producing a curved profile shape that eliminates any shockwave generation and thus doesn't allow any pressure drop to occur. Several conceptual designs are possible as far as the profile shape is concerned.

This configuration is basically similar to the de Laval nozzle and it also resembles the Venturi nozzle design. These two configurations are basically used to accelerate pressurized gases passing through them at supersonic speeds. The de Laval nozzle on its expansion is basically performing in such a way as to convert the energy propelling gas into directed kinetic energy. Because of this, the de Laval nozzle is used in steam turbines, and in modern rocket engines. It's also used in supersonic jet engines.

Therefore, it is not the configuration that is claimed here but its operational usage that is unique. This is true because in all cases mentioned before (De Laval & Venturi) there is no piston head at the exit of the nozzle. The converging diverging nozzle in this case is being used to provide kinetic energy inside the pneumatic engine by using compressed stored air as propellant, while the de Laval nozzle is used to transform a propellant mass to kinetic energy to move entire jets or rocket designs.

Operation of Pneumatic Engine

1. Compressed air is injected and accelerated through the CDN into the piston chamber.

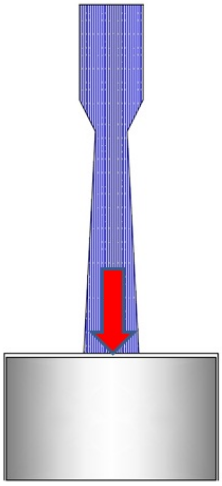

   a. One piston is at TDC with its cam wheel resting just above the trilobe
   b. The other piston is at BDC with its cam wheel pressed against the trilobe base

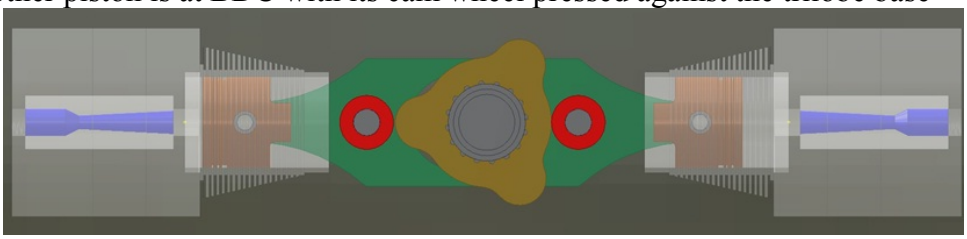

2. Incoming airflow quickly pressurizes the piston chamber and exerts a force on the piston causing it to displace, expanding the piston chamber

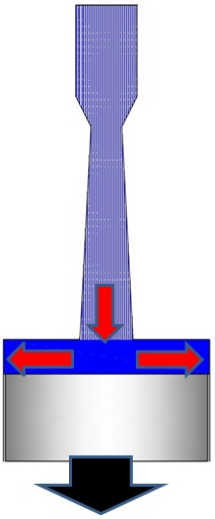

   a. One piston chamber is pressurized with its cam wheel pressed against the top of a lobe, exerting tangential forces to induce rotation

b. The other piston chamber is contracting with its cam wheel translating away from the trilobe base

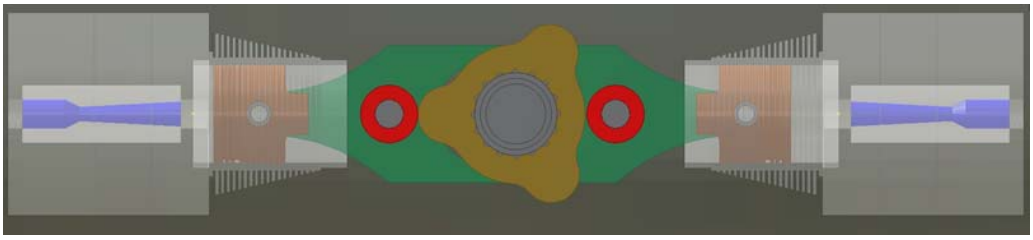

3. The piston displaces to BDC where the exhaust ports become uncovered and air is accelerated out of the piston chamber

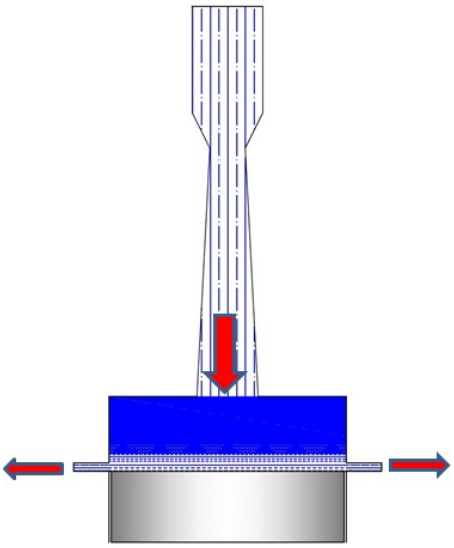

a. One piston chamber is exhausting the air with its cam wheel in the trilobe divot (the area between the lobe and the trilobe base)
b. The other piston chamber continues to contract with its cam wheel completely free from any contact

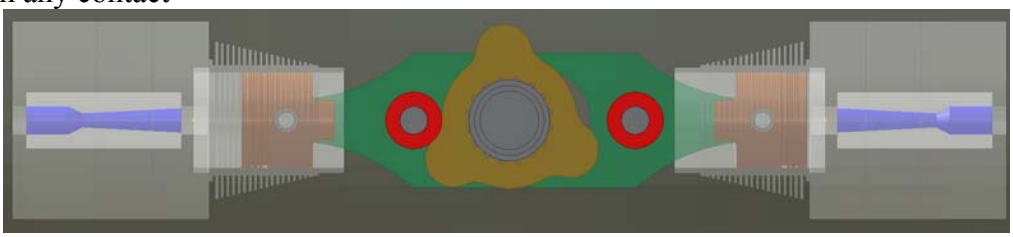

4. The exhaust process lowers the pressure in the piston chamber and the piston begins its return to TDC

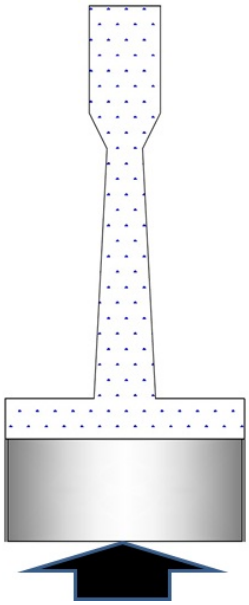

a. One piston is at BDC with its cam wheel pressed against the trilobe base
b. The other cylinder is at TDC with its cam wheel resting just above the trilobe
    i. This cylinder begins the cycle the other cylinder just completed

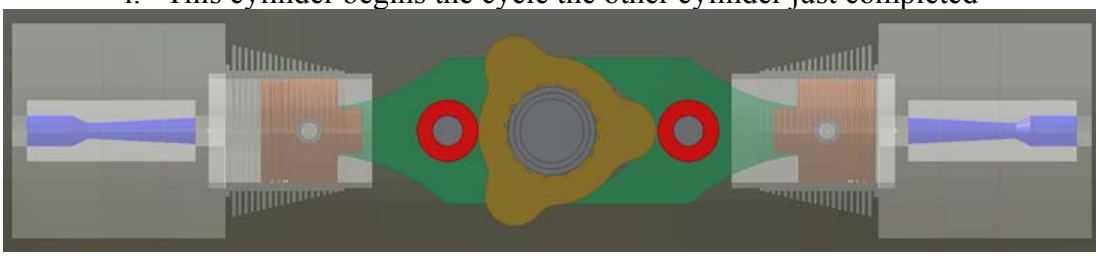

Engine Dynamics

Given the desired or predicted force that will be exerted on the piston, the torque of the output shaft of the pneumatic motor the Virtual Work Equation from machine dynamics is used:

(1) $\Sigma \mathbf{F} \cdot \mathbf{V} + \Sigma T\omega = \Sigma m\mathbf{A} \cdot \mathbf{V} + \Sigma I\boldsymbol{\alpha} \cdot \boldsymbol{\omega}$

Where bold characters denote a vector and "·" denotes the vector product. Using this equation the output torque "T" is calculated as a function of the input force F. To do this the mass, moment of inertia, center of gravity and velocity and acceleration profiles of all the components of the engine assembly must be known. The mass of the trilobe shaft may be neglected since it is moving in purely rotational motion and will have a zero linear velocity and acceleration. The center of gravity for each piston should be at the connection points to the connecting rod. The center of gravity for the connecting rod should be at its middle since it is symmetrical. The term

$I\boldsymbol{\alpha} \cdot \boldsymbol{\omega}$ for the pistons and connecting rod may be neglected since they are not rotating, but simply translating horizontally. This term may also be neglected for the trilobe shaft since it will be rotating with a constant angular velocity (zero angular acceleration).

To acquire the velocity and acceleration profiles of the components, realize that the connecting rod will always stay in contact with the camshaft and so it will move horizontally at the same rate as the radius of the camshaft in the plane of the connecting rod changes. This requires an equation for the rate of change of the radius of the camshaft to give the equation for the linear velocity of the connecting rod and therefore the attached pistons as well. To do this, 108 points along the perimeter of the camshaft should be measured to get a relationship between the radius of the camshaft in terms of the angular position of the camshaft. This data should be used as an input to generate and equation by using an eighth order Fourier regression of the data points.

Using this equation for radius in terms of position, take the derivative to get the velocity as a function of position and angular velocity. Taking the derivative again gives the equation for the acceleration profile as a function of position, angular velocity, and angular acceleration.

Finally, the Virtual work equation can be solved for the equation for the output Torque T, where links 1 and 2 are the pistons and link 3 is the connecting rod.

(2) $T=(m_1\mathbf{V_1}\cdot\mathbf{A_1} + m_2\mathbf{V_2}\cdot\mathbf{A_2} + m_3\mathbf{V_3}\cdot\mathbf{A_3} - \mathbf{F}\cdot\mathbf{V})/ \omega_{camshaft}$

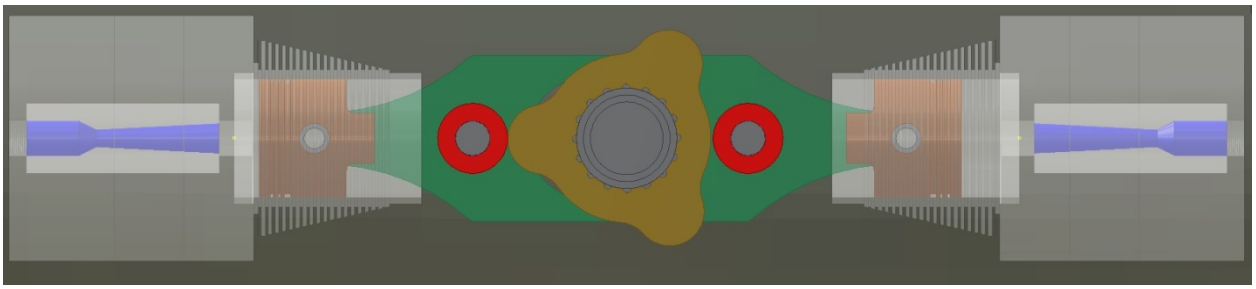

Figure 1. Initial CAD Design of pneumatic engine

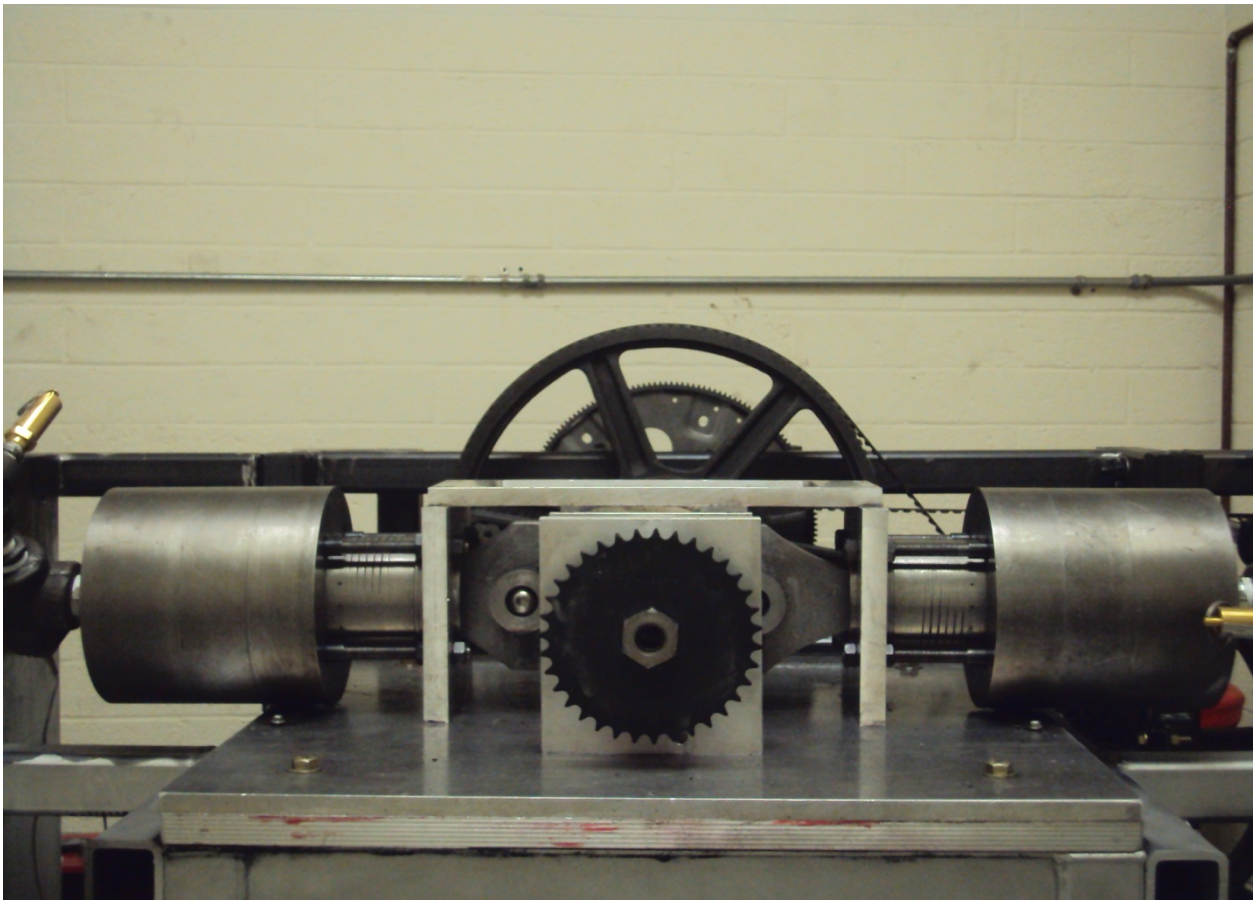

Figure 1. Final Assembly of pneumatic engine

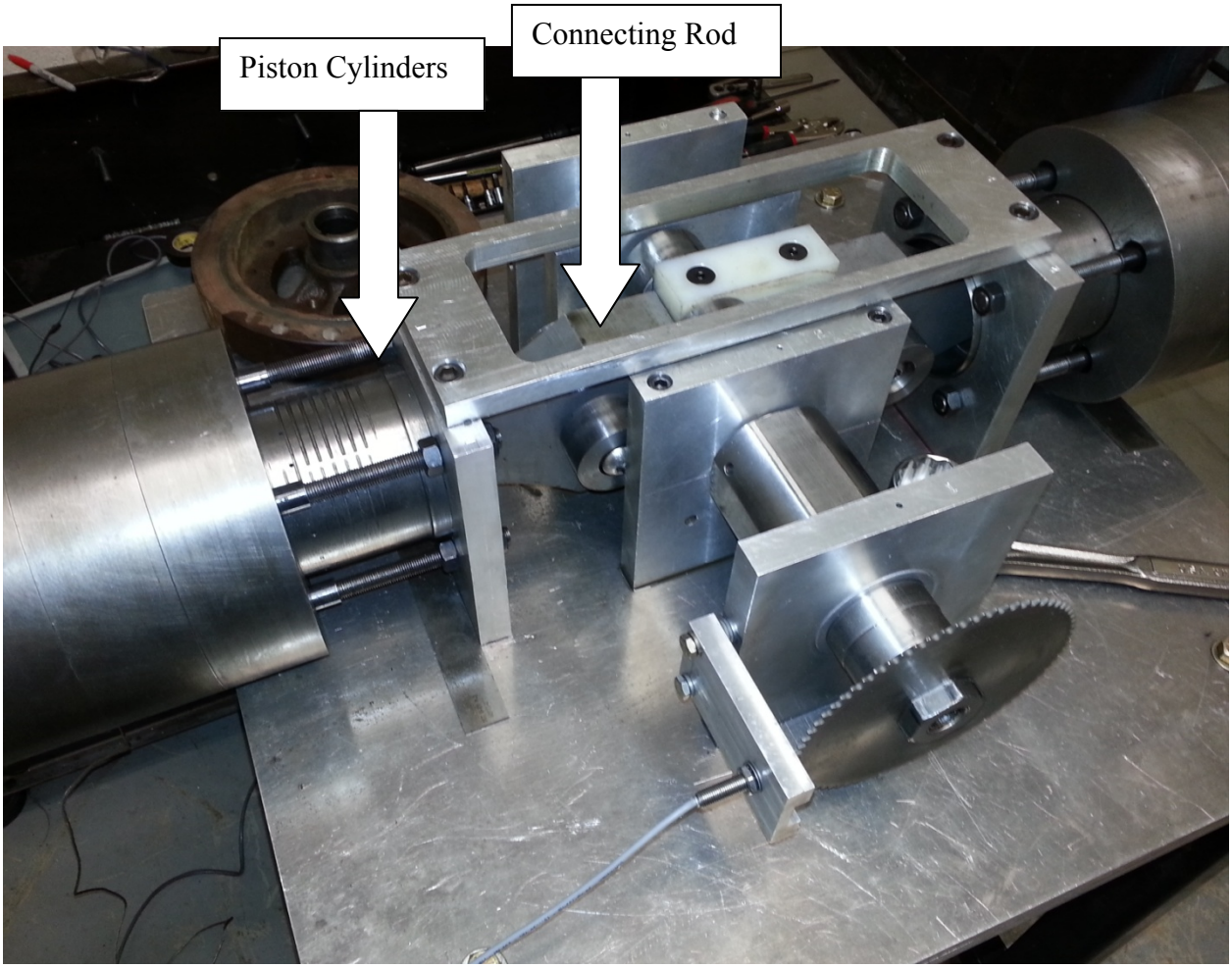
Piston Cylinders
Connecting Rod

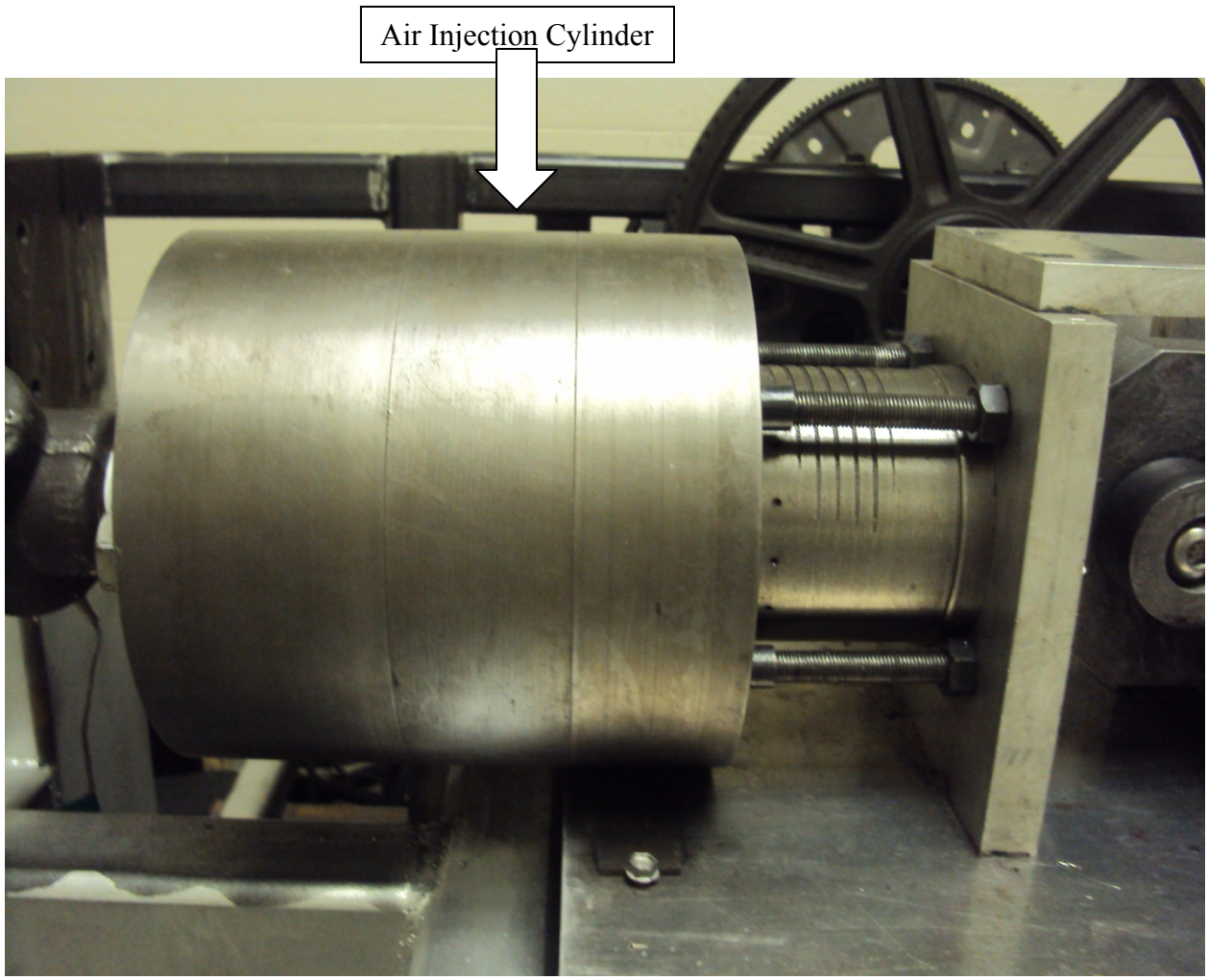
Air Injection Cylinder

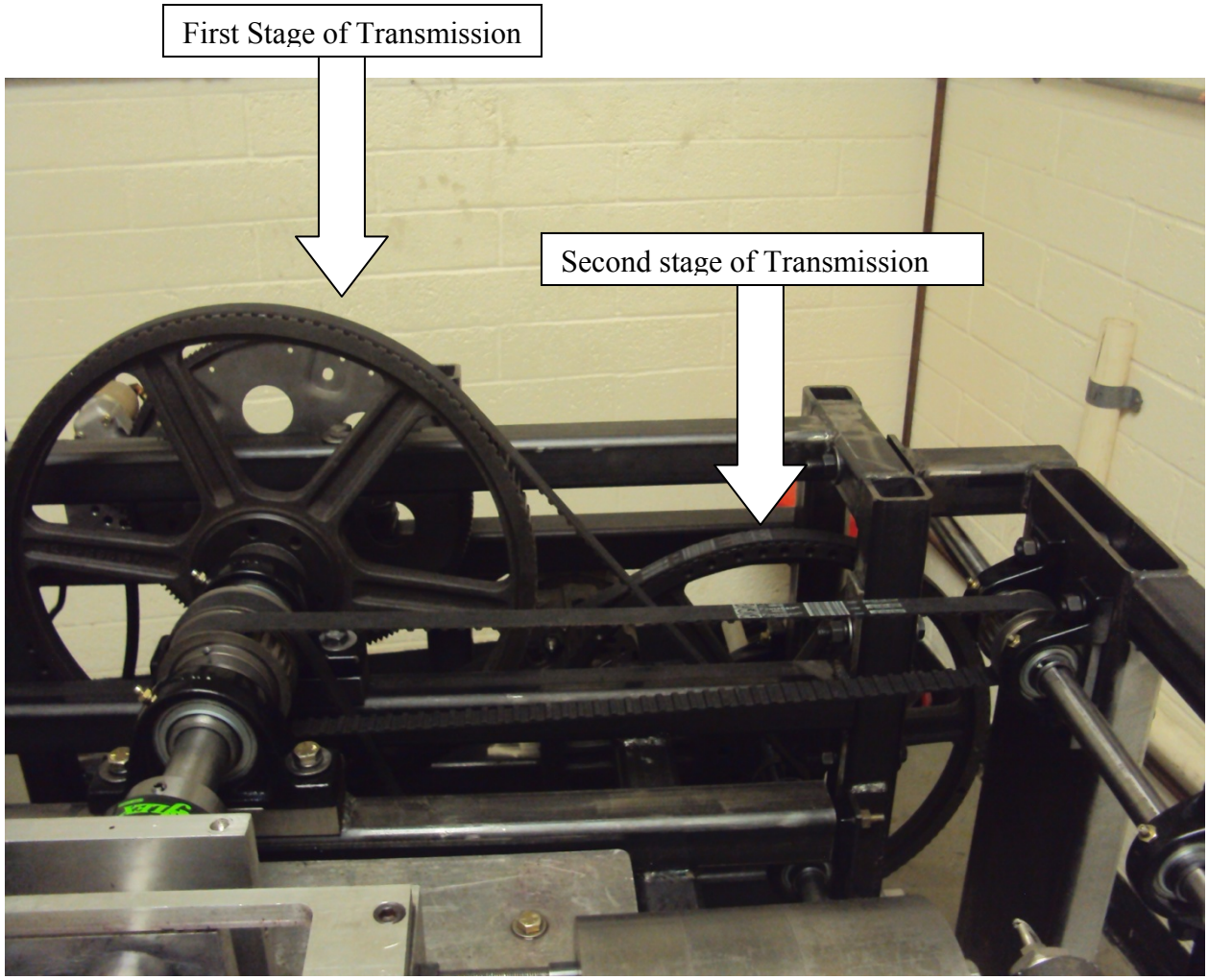
First Stage of Transmission
Second stage of Transmission

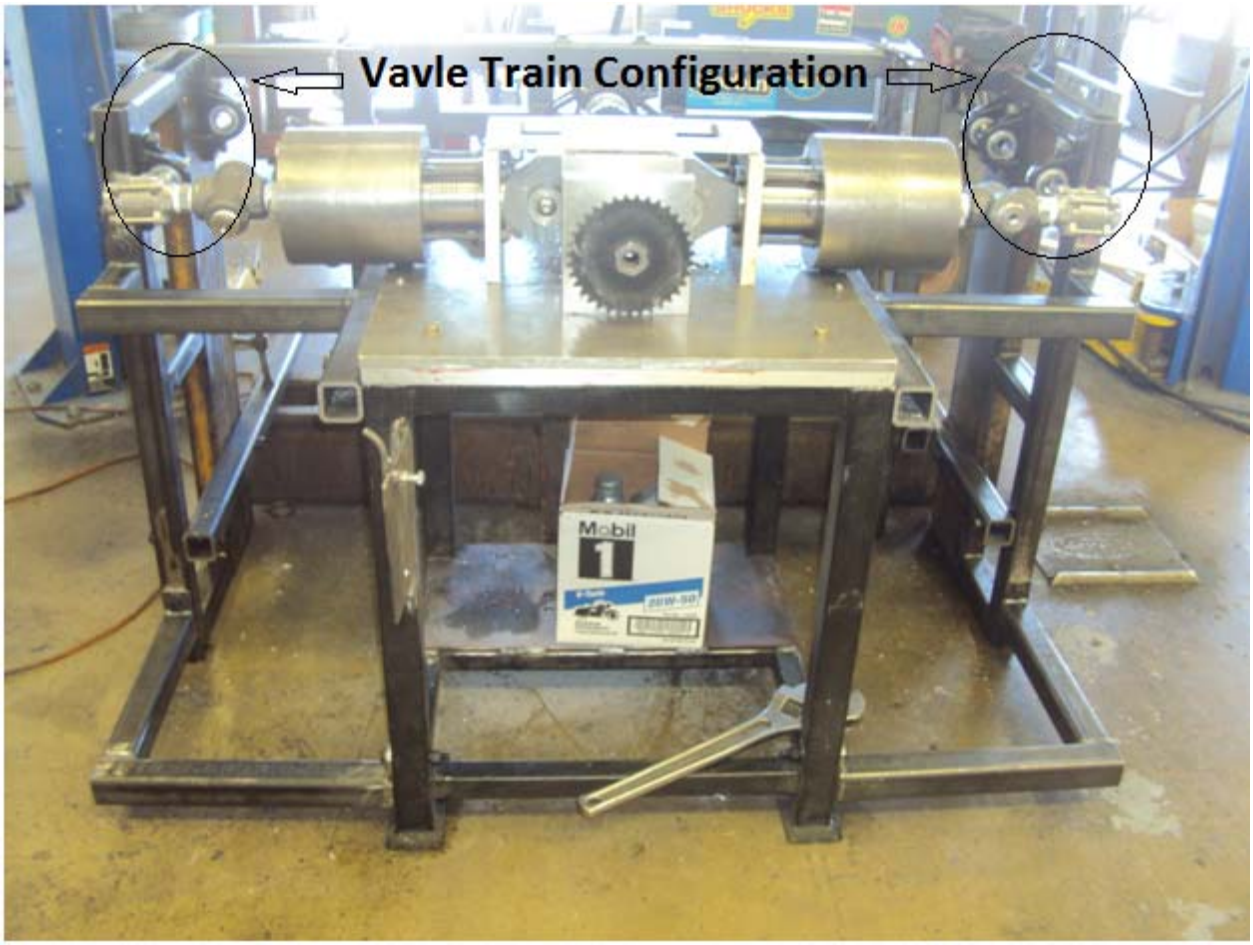
Vavle Train Configuration
Mobil
1

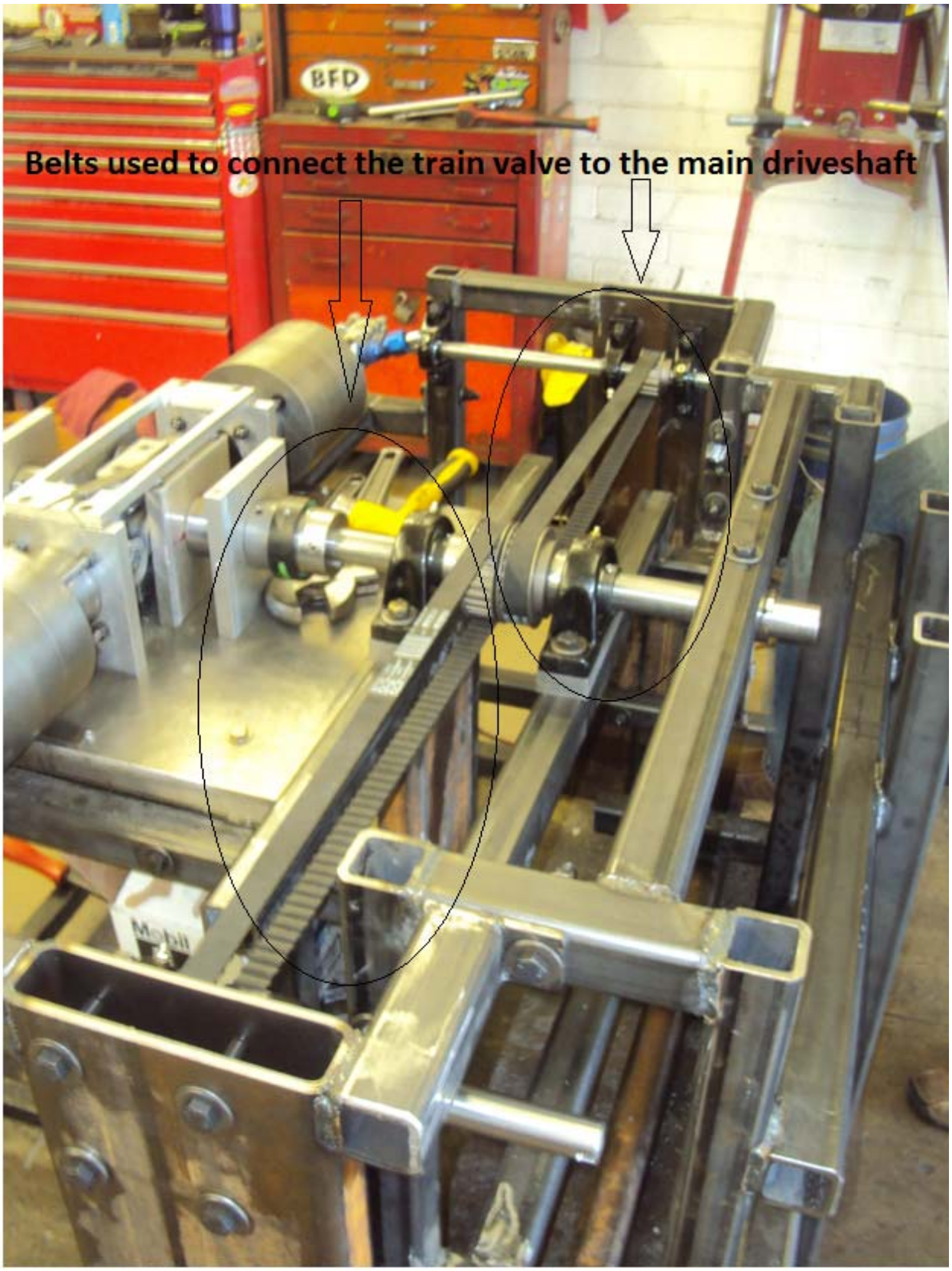
Belts used to connect the train valve to the main driveshaft
BFD

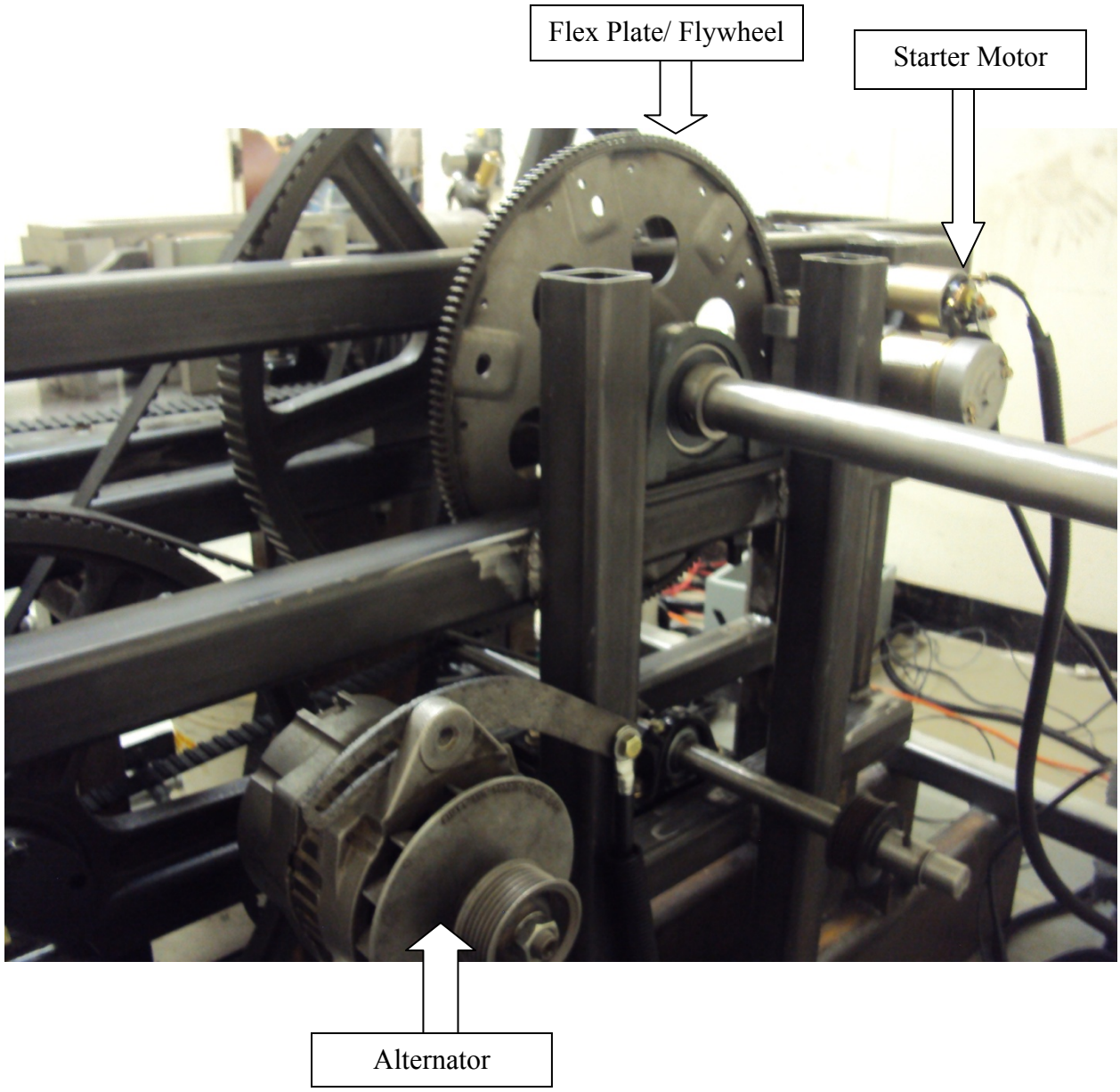
Flex Plate/ Flywheel
Starter Motor
Alternator

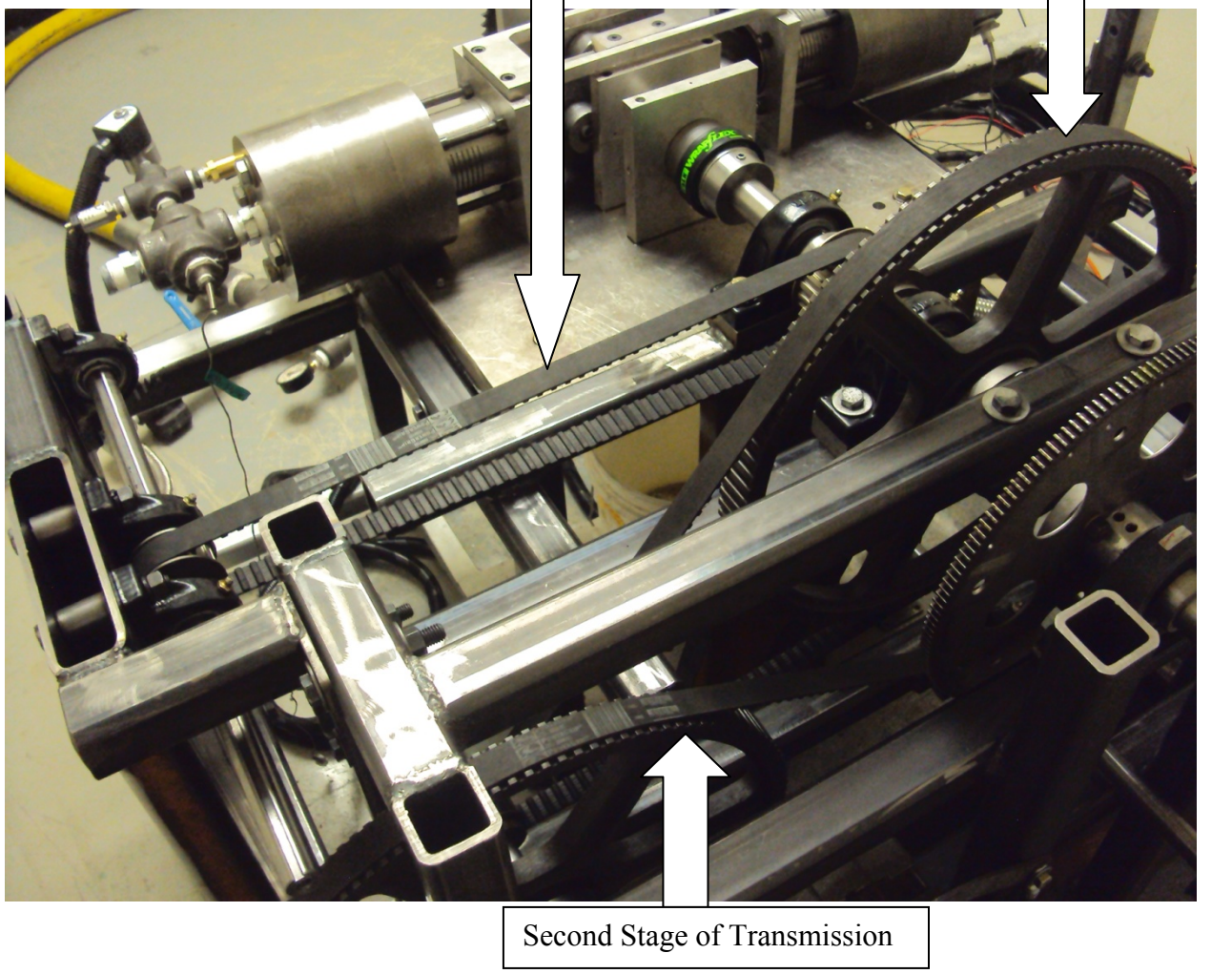
Belts used to connect main driveshaft to valves
First stage of Transmission
Second Stage of Transmission

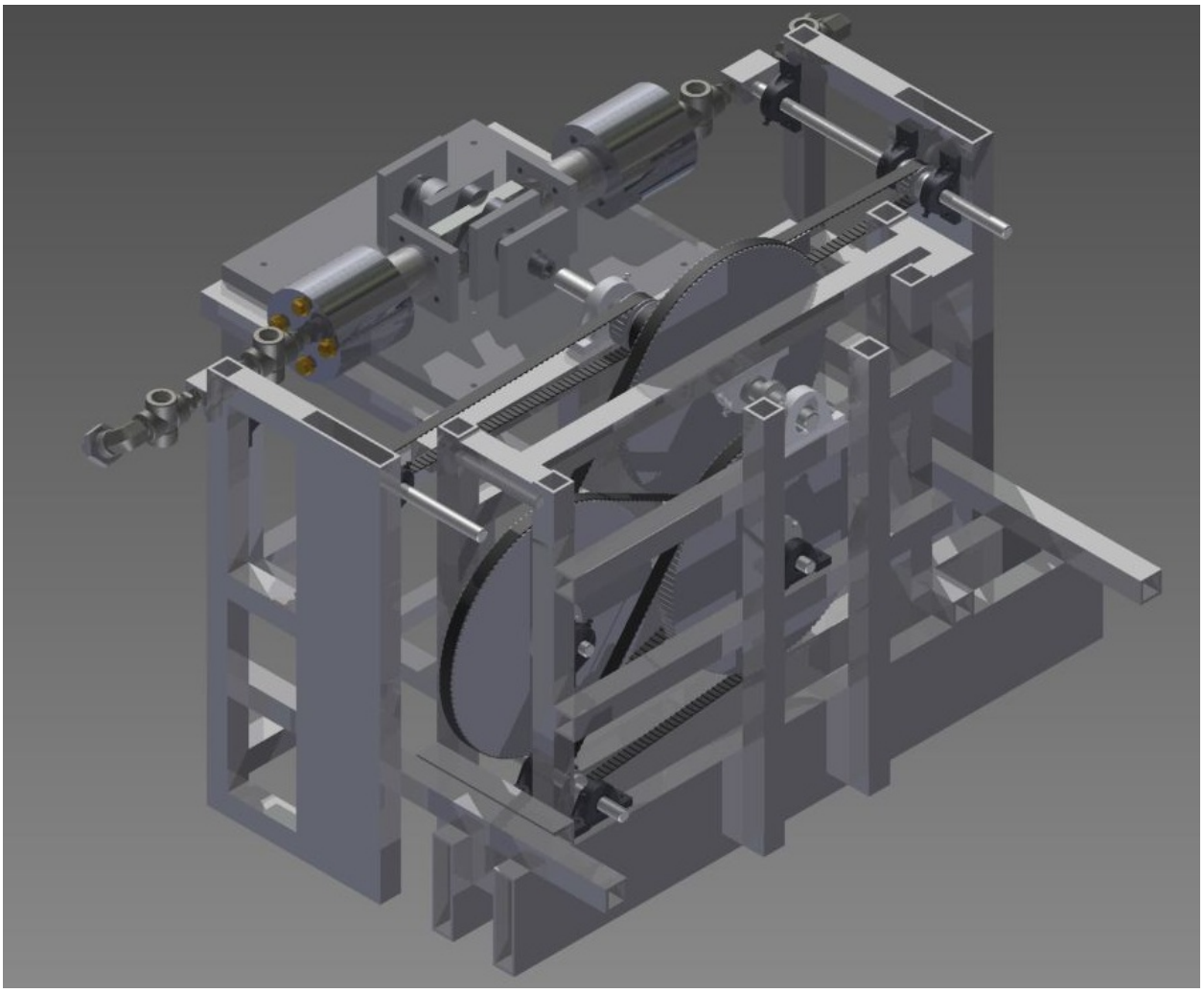

Figure 3. CAD Rendering of Complete Engine Assembly

Supersonic Converging Diverging Nozzle Simulation and Experimentation, Method of Characteristics and Design of Various Nozzle Profiles

Compressed Air Energy Storage consists of three stages. This report concentrates on the third stage which is basically when energy extraction occurs. Particularly, the first part of the report goes over the design, simulation and experimentation of a particular converging diverging nozzle design. The converging diverging nozzle is a major part of the pneumatic motor, which is being used for the expansion process of CAES. It is essential to mention that the reason that the converging diverging nozzle configuration was selected was that it efficiently expands the stored compressed air while it produces a great amount of force to move the piston heads of the motors. A thermodynamic analysis of the CAES piping system is also part of this reports, as well as a

brief discussion on the engine dynamics of the pneumatic motor used for the energy extraction in the third stage of CAES.

The first part of the report is divided in two parts. The first half deals with the optimization and simulation of the flow conditions in the converging diverging nozzle while the second half deals primarily with the experimentation performed towards the characterization of the converging diverging nozzle. Towards the end of this report, a brief discussion will be made on the findings of the research conducted towards the third stage of CAES, as well as a comparison between experimentation and simulation regarding the converging diverging nozzle will be made.

Simulation

The simulation of the converging diverging nozzle was performed using different software packages. This was done in order to ensure the validity of the results. The approach that was taken in this direction was to perform Computational Fluid Dynamics analyses so that an extensive amount of information would be provided as far as the flow characteristics of the third stage of CAES are concerned. Also, the Computational Fluid Dynamics analyses gave an idea on what it should be expected during the experimentation process. COMSOL and MATLab were two of the programs used in order to develop all the appropriate Computational Fluid Dynamics codes required to complete the simulation part of this research.

COMSOL was primarily used to ensure that the designed velocities and thrust values were able to be predicted by this software package but also to obtain some temperature and pressure values that could not be solved analytically but rather using an advanced software. As it can be seen in the following graphs Mach numbers and flow temperatures are some of the outputs that this software package was able to provide. In the first figure below it can be seen that for a given inlet pressure, the converging diverging nozzle is able to achieve a supersonic speed and more particularly Mach 1.53. It must be noted that the speed achieved is dependent on the inlet pressure conditions. The higher the inlet pressure, the higher the speed that will be achieved. The thrust produced by the nozzle is dependent on the velocity that is achieved at the exit plane of the converging diverging nozzle. Therefore, increasing the pressure at the inlet will ultimately increase the thrust at the exit plane, given that there are no abruptions in the flow conditions that are not taken into account. The simulation was able to validate the fact that by increasing the inlet pressure, which is basically the pressure at which the air is stored, the velocity and thrust increase at the exhaust of the converging diverging nozzle.

Figure 1. Case 1. Inlet Pressure 110 (psi)

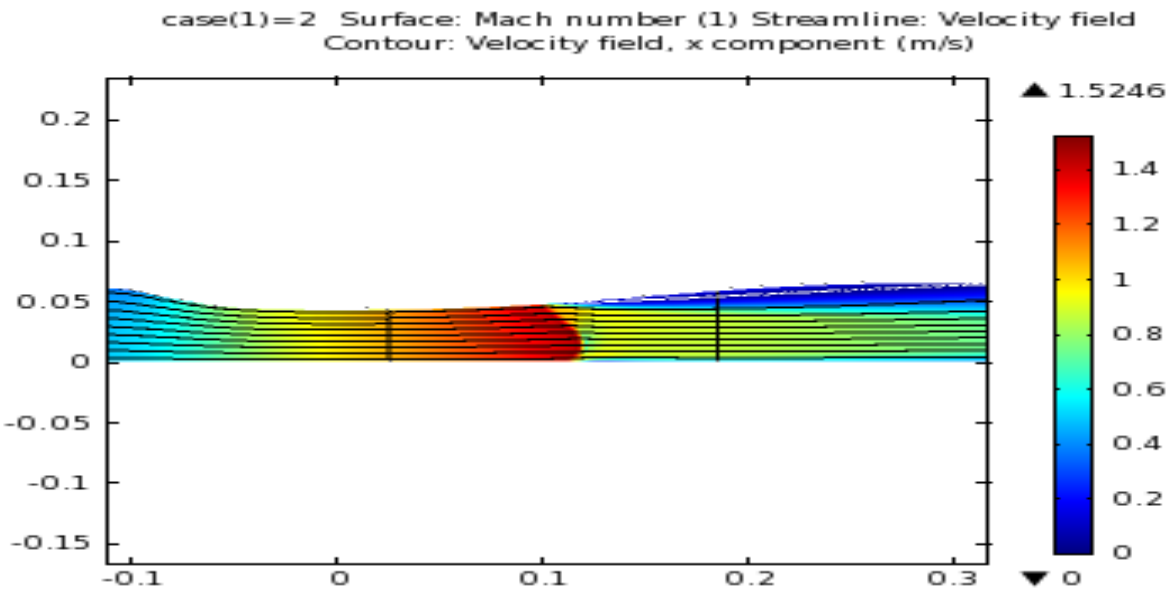

The figure below is showing the drop in temperature across the converging diverging nozzle. Occurrences like that are expected simply because as the velocity increases and thus the air is expanded in higher Mach numbers, the temperature will drop to very low values.

Figure 2. Case 1. Inlet Temperature 260 (K)

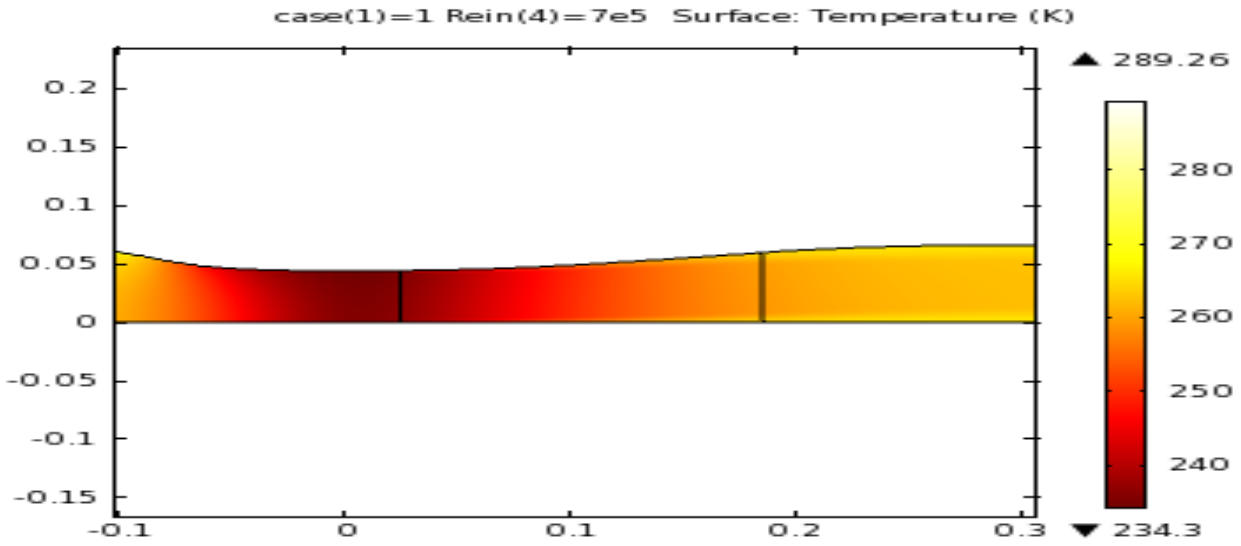

Another case was considered in the simulation process. This was in a much lower pressure region of 45 psi. As it can be seen by decreasing the inlet pressure the velocities are decreased significantly. The reason for this is that in the converging diverging nozzle design the amount of thrust and velocities reached are dependent upon the inlet pressure. This dependency that the converging diverging nozzle has on inlet pressure is what makes it the most suitable element in expanding compressed stored air, which is usually stored in high pressure regimes. As it is already explained, because of the low inlet pressure the following graphs show a case that

the velocities don't reach supersonic velocities. At this point it is essential to mention that the fact that at low pressure ranges the converging diverging nozzle drops in subsonic velocities does not imply that the thrust produced is decreased significantly. On the contrary, when subsonic speeds are reached, shockwaves cease to exist to the extent they occur in the supersonic cases. Shockwaves cause pressure drop and thus trigger losses in the thrust produced and thus it is beneficial to avoid the occurrence of any shockwaves. Therefore, even if the speed is subsonic, the amount of thrust produced is still capable of providing enough force to move the piston heads.

Figure 3. Case 2. Inlet Pressure 45 (psi)

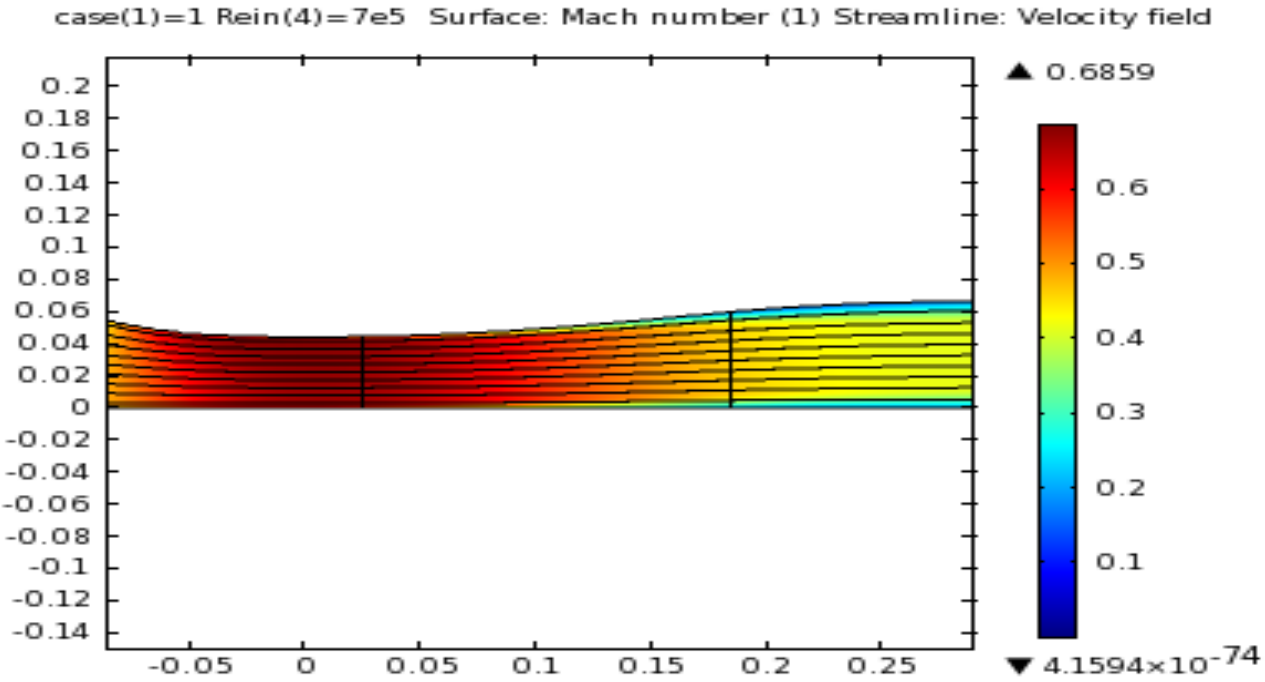

The temperature readings below, reach a low of 248 Kelvin. In the previous case the lowest temperature reached was 234 Kelvin. This proves the point that as the velocity is increased the temperature is decreased. Also, at this point another relationship can be determined; as the inlet pressure was increased and this the exit velocity increased, the temperature was decreased. The computations of the temperature drop were verified in the experimentation process, where a thermocouple reached a low temperature of 253 Kelvin (-20 Celsius). The fact that this temperature was recorded during experimentation shows that the simulation has proved to be providing predictions that are very close to what the realistic numbers are. It is essential to mention that all these simulations were performed for a variation of Reynolds numbers. This was conducted in order to incorporate the effects of Reynolds number in the Computational Fluid Dynamics analyses.

Figure 4. Case 2. InletTemperature 270 (K)

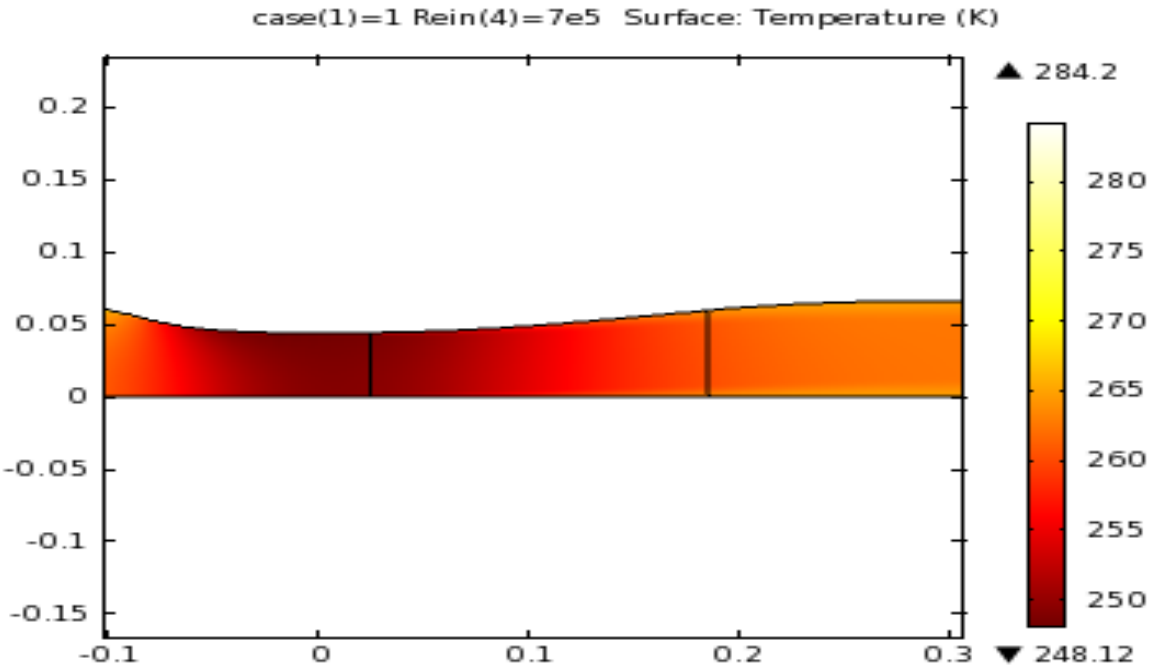

Figure 5. Case 2. Variation of Static Pressure

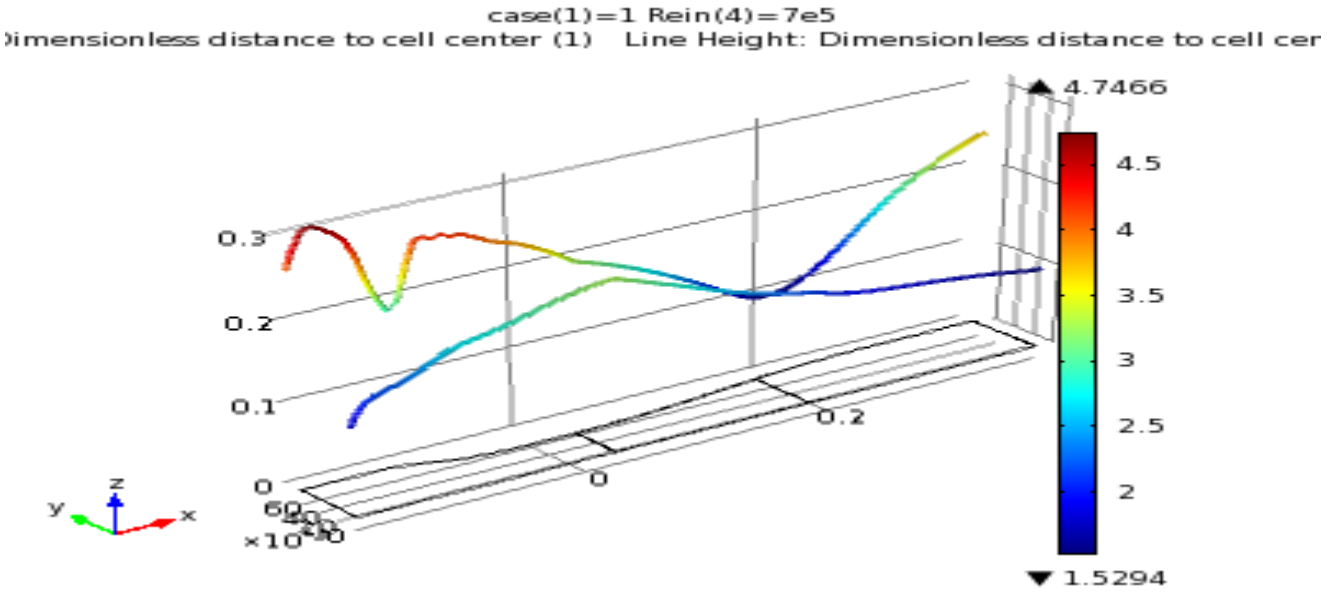

As mentioned earlier, MATLab was also used to obtain some results regarding the converging diverging nozzle design and simulation. Two different codes were used, in order to make computations regarding various parameters of the converging nozzle. The first code was able to output essential information that was used in the design process. It was made possible to predict the Mach number through a CFD analysis.

Figure 6. Thrust Curve of Converging Diverging Nozzle

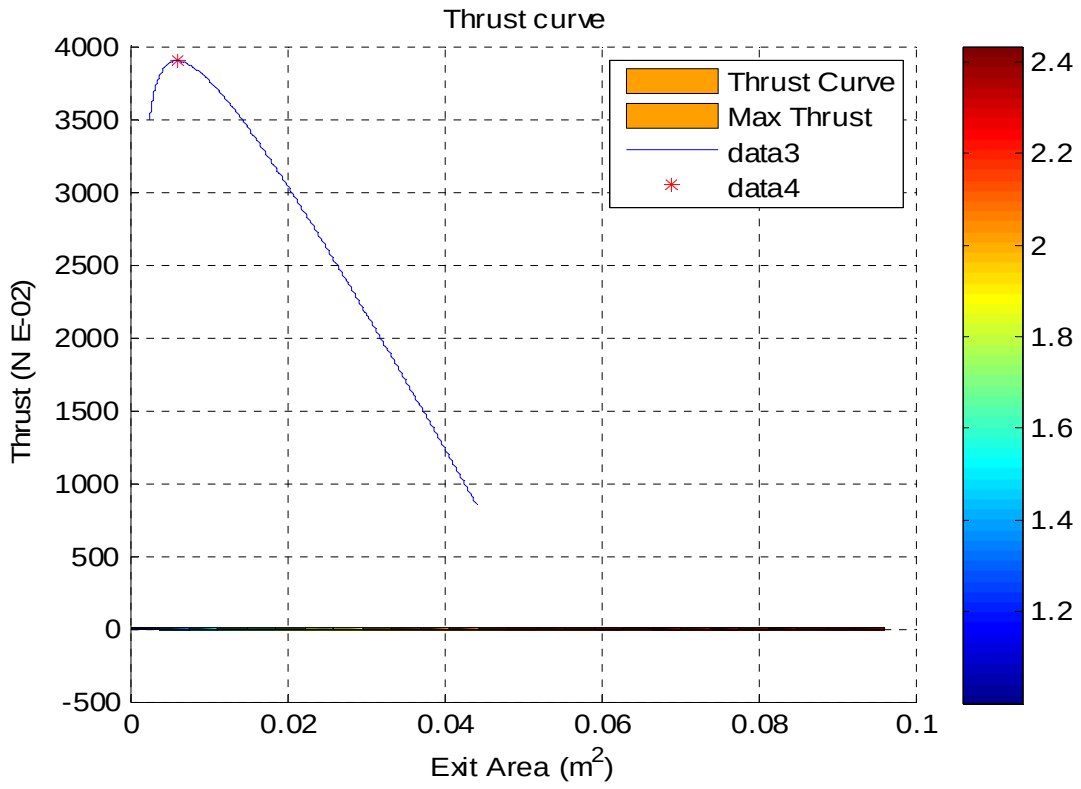

In the figure above a thrust curve was able to be produced based on the design specifications of the manufactured converging diverging nozzle, which was later used in the experimentation process. The figure contains the maximum thrust point and also the point in the converging diverging section that it's occurring. The information obtained from this graph was essential in continuing the simulation process, as the location that the maximum thrust occurs had to be defined, prior to finalizing the shape and inlet conditions of the converging diverging nozzle. As it will be shown, similar shapes of thrust and pressure curves, as shown above, were produced using experimentation data.

In order to properly conclude on a specific converging diverging nozzle design and be able to determine the behavior of the flow inside this specified geometry element, MATLab was used to provide essential information about the existence of shockwaves within the nozzle, determine the length of the nozzle, the throat of the converging area, the variation of the Mach number within the nozzle, the variation of the pressure ratios throughout the nozzle design, as well as the pressure ratio and Mach number at the exit. As it can be seen in the second graph of the following figure, the exit Mach number that this code was able to predict was around Mach 2.5. It will be shown that this number was very close to the Mach number measured during experimentation. Also the pressure ratio at the exit here is given to be around 0.05, which is very close to the Mach number when solving for it using the isentropic flow equations. This will also be shown to match very accurately to the pressure ratio that was obtained during the

experimentation process. Therefore, the simulation process was able to predict accurately the conditions that should be expected in

Figure 7. Nozzle Design

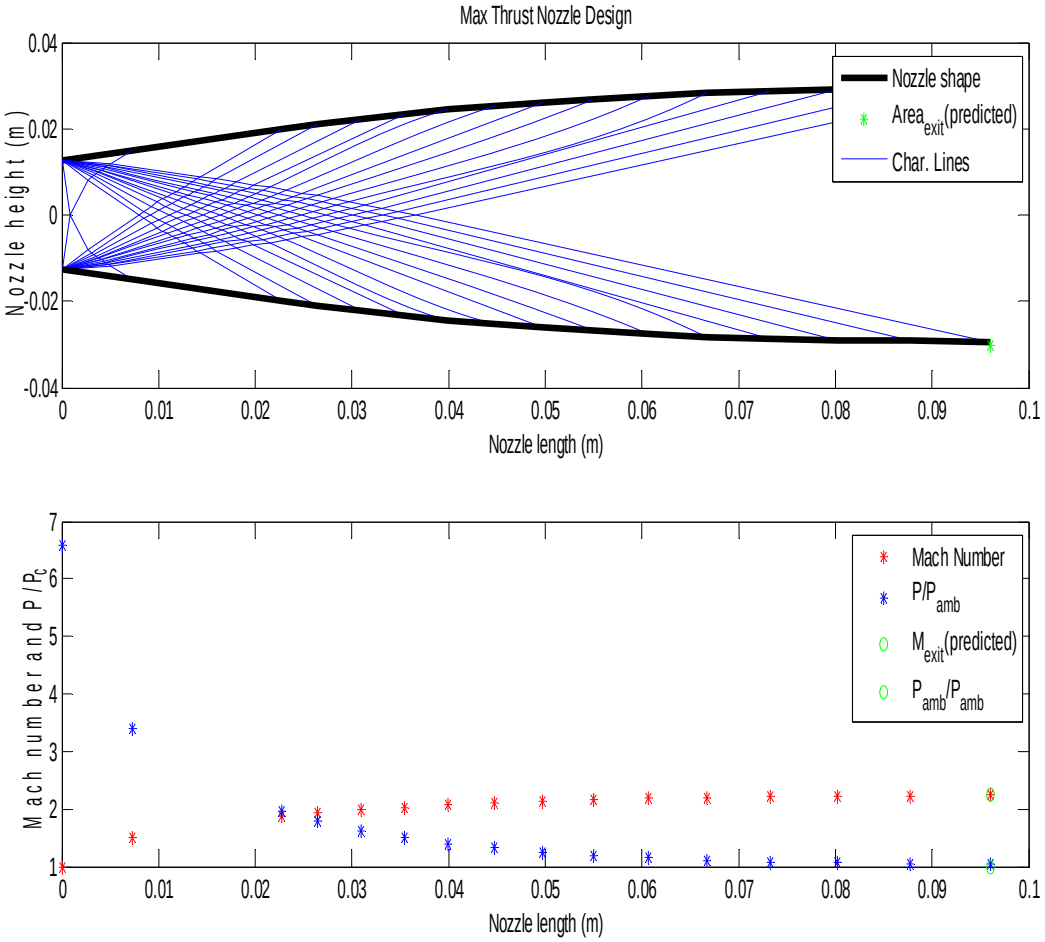

Once the dimensions and inlet conditions were finalized in the design process, based on the information that the simulation has provided, a Computational Fluid Dynamics analysis code was run to predict the exit Mach number. Following is a figure that was obtained through this CFD analysis and shows the behavior of the flow velocity inside the diverging section of the nozzle. It is simply describing the fact that the converging diverging nozzle is capable of reaching high supersonic speeds for a given inlet pressure. In this particular case the pressure in the stored tank is assumed to be at 500 psi. The pressure drop across the piping and piping components that are connecting the tank to the converging diverging nozzle was calculated to be around 45 psi, and thus the actual inlet conditions are 450 psi. The pressure drop across the nozzle should be around 300 psi, which actually yields a pressure ratio of the ambient pressure over the exit pressure of around 0.047. Consequently, the pressure ratio resulted in a Mach number that reached its maximum value at the exit plane of the nozzle. As shown below, this

number reached a little above Mach 2.4. Therefore, the fact that air is stored at that high pressure ranges allows for achieving high Mach number and accordingly a higher amount of thrust at the exit plane of the converging diverging nozzle.

Figure 8. Mapped Mach number variation across CDN

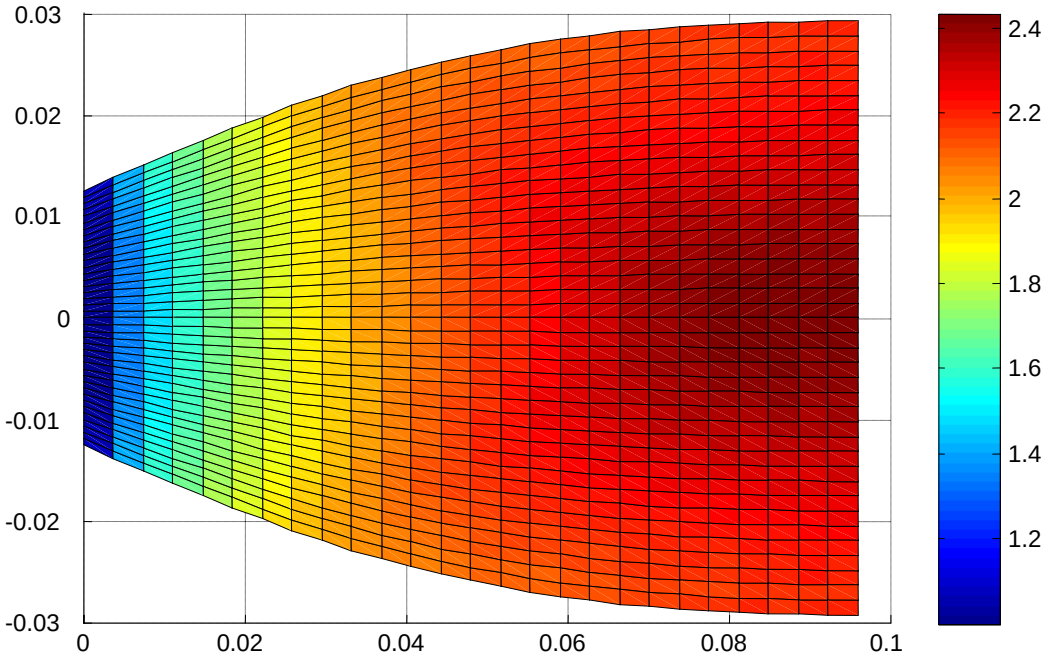

The second code that was developed in the process of the simulation was aimed towards providing a significant amount of data regarding the conditions at the inlet, throat area and exit plane of the converging diverging nozzle. Different flow conditions were considered in order to compute and simulate any possible outcome that the usage of a converging diverging nozzle configuration could have. As it is shown below and as it was mentioned earlier the pressure ratios achieved in a converging diverging nozzle are determining factors about the thrust, Mach number, mass flow rate and temperature variation that is experienced when flow goes through the converging and diverging section of the nozzle. Taking advantage of that fact, this code was build to categorize different cases based on the inlet and exit pressure variation. The information that this code provided was very useful because it covered all of the properties and values that would be required to characterize the converging diverging nozzle at least from a simulation standpoint. These data were later compared with the experimentation data and it was verified that simulation was very close to the experimentation results.

Following is the criterion based on which the cases in the MATLab code were categorized. As it can be seen the criterion is the pressure at the exit (Pb) of the converging

diverging nozzle over the total pressure (Po). It must be noted here that the total pressure is the one that will create a force on the piston heads of the pneumatic engines. Therefore, the greater the total pressure the higher the force. For that reason the pressure ratio is desired to be as small as possible.

Pb/Po Regions

Subsonic 1.000000 > Pb >= 0.973182

Normal Shock 0.973182 > Pb >= 0.375959

Oblique Shock 0.375959 > Pb > 0.047299

Supersonic Design Pb = 0.047299

Prandtl-Meyer 0.047299 > Pb >= 0.000000

Table 1. Converging Diverging Nozzle Cases

Prandtl-Meyer Case	**Oblique Shock Case**	**Subsonic Case**	**Normal Shock Case**
Me = 2.6374	Me = 2.6374	Me = 0.1905	Me = 0.2398
Pe = 47.2987 KPa	Pe = 47.2987 KPa	Pe = 975.0000 KPa	Pe = 800.0000 KPa
Te = 135.0790 K	Te = 135.0790 K	Te = 320.6720 K	Te = 319.3289 K
Ve = 614.4373 m/s	Ve = 614.4373 m/s	Ve = 68.3889 m/s	Ve = 85.8790 m/s
Mass flow rate = 0.3499 Kg/s	Mass flow rate = 0.0148 Kg/s	Mass flow rate = 0.0014 Kg/s	Ms = 1.7544
Thrust = 181.4196 lbs	Thrust = 107.8196 lbs	Thrust = 18.0974 lbs	Shock Location = 1.3910
			Mass flow rate = 0.0017 Kg/s
			Thrust = 78.7565 kN

Based on the outputs of this code it was decided that the best case that had to be followed was the oblique shock case, since the Thrust output was sufficient for the engine operation and at the same time there was no sacrifice in a high value for mass flow rate.

Values before Oblique Shock

Me = 2.6374

Pe = 47.2987 KPa

Te = 135.0790 K

Ve = 614.4373 m/s

Mass flow rate = 0.0148 Kg/s

Thrust = 107.8196 kN

At this point a comparison between COMSOL and MATLab was made in order to ensure the validity of the results. Temperature computations seemed to be in agreement since for the supersonic oblique shock case, both programs gave an answer around 135 K. In particular, COMSOL's answer was 138 K while MATLab gave 135 K. The Mach number predictions

match very well for both simulation programs, since MATLab gave an exit Mach number of 2.64 while COMSOL provided an exit Mach number of 2.53.

Experimentation

The experimentation was performed mainly towards the characterization of the manufactured converging diverging nozzle. One of its objectives was to explore the variation of the back pressure in the converging diverging nozzle. The variations of back pressure are caused by the moving boundary of the piston head. The analysis was as vital as the experimentation, since safe conclusions can be drawn if the data are analyzed properly. The analysis procedure was also done using a MATLab code to minimize the time of computations and ensure the validity of the results. The two sets of experiments that were performed were with a LoadCell to measure the thrust at the exit of the converging diverging nozzle and a pitot tube, a device that is widely used in wind-tunnels and aircrafts to measure the velocity. Therefore the overall plan for this experimentation would be to first perform the LoadCell and pitot probe experiments and then perform analysis on these two experiments.

Before reviewing the results from the experimentation, it is essential to mention briefly some general information about these sets of experiments. Starting off with the pitot tube experiments that had as a primary objective to characterize the velocity of the flow through the converging diverging nozzle. A pitot static probe was used to measure the static and total pressure at the exit of the converging diverging nozzle. Using the static and total pressure measurements the velocity was calculated at the test section. The data that were collected during the experimentation were later used in the analysis process to determine the maximum possible velocity that was achieved at the exit of the CDN. Also the thrust exerted on the piston head, the optimum pressure regime for operating the CDN were also computed based on the data that were collected in the experimentation process. Finally, the velocity profile over a wide of inlet pressures was computed and also a comparison was made with the LoadCell data.

The experimentation was performed over a wide range of inlet pressures in order to determine when and where the speed of the flow exiting the converging diverging nozzle reaches supersonic speeds. The pitot static tube experiments proved that the designed converging diverging nozzle was capable of reaching supersonic speeds. One indication is the figure below. As the stagnation pressure increases, the static pressure drops below atmospheric, indicating the existence of a shock in front of the pitot static tube. As the static pressure reaches atmospheric values again, it indicates that the converging diverging nozzle is returning to subsonic velocities. In the plot below, the pressure ratios are indicating the Mach number reached at the exit of the nozzle. As the pressure ratio increases, the Mach number increases as well. The highest Mach number reached according to the pitot tube experiments was at 500 psi inlet pressure, which was the highest inlet pressure. The corresponding Mach number for 500 psi inlet pressure was 2.67. Following is the velocity profile of the converging diverging nozzle, as described by the pitot tube experimentation results.

Figure 9. Pressure Ratios

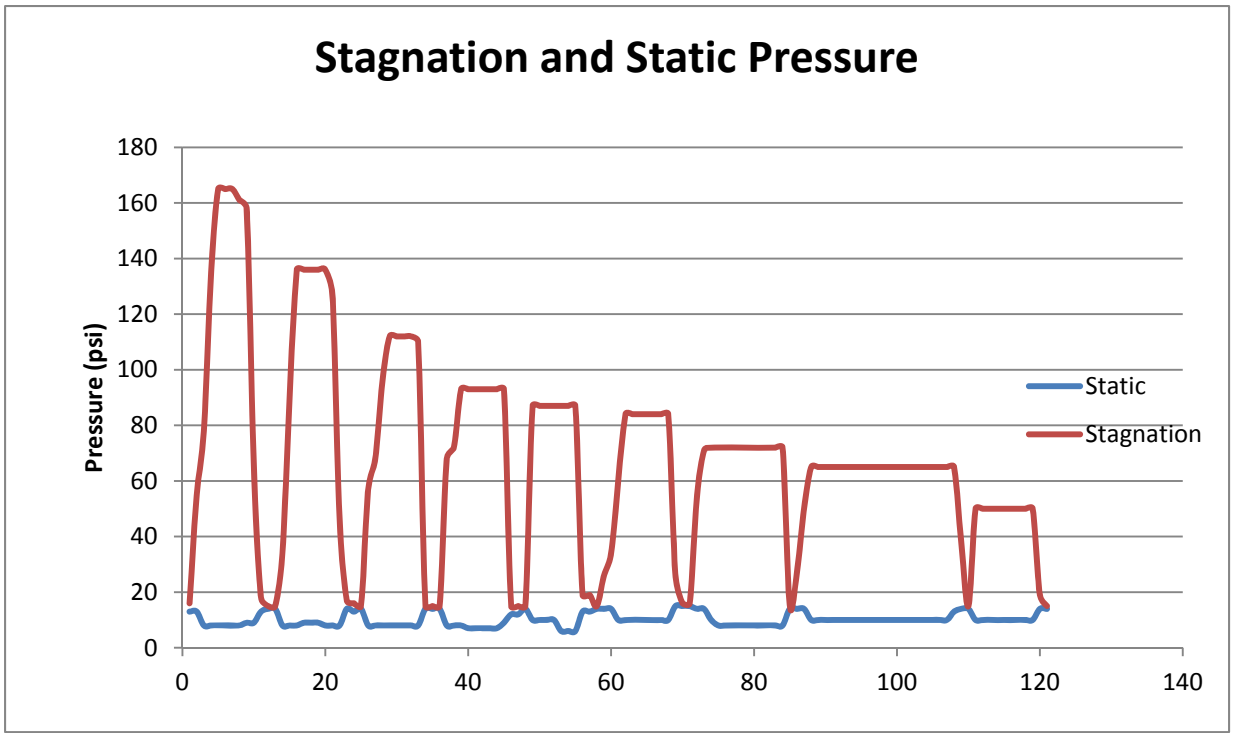

Another observation that should be made when looking at this graph is that the overall pressure and Mach number drop is not a rapid one. In other words there is no indication of a cutoff pressure value where the pressure ratio starts becoming extremely large or hit extremely small values without any previous indication. This simply means that the Mach number will eventually drop as the pressure will drop, but it will not cause any unexpected behavior on the converging diverging flow velocities.

In the figure below, the stagnation and the thrust curve are plotted in order to confirm that as the stagnation pressure drops smoothly throughout the pressure range, the thrust curve follows the same pattern. This is simply happening because the stagnation or total pressure is multiplied by the exit area of the nozzle to determine the thrust produced on that area. Because of the exit area being small, the thrust curve will be a vertical shift downwards of the stagnation pressure drop. This indicates that by making the area of the converging diverging nozzle at the exit larger, there is a benefit of producing a higher thrust. This is something that will be incorporated into the next designs. Also the numbers of the stagnation and the thrust curve seem to be in agreement with the numbers produced by the LoadCell experiments, which will be discussed later in the report. The highest amount of thrust obtained during the pitot tube experiments was 107 lbs, a number that matches the MATLab predictions very close. Also, as mentioned the Mach number reached was 2.67 while the prediction in the simulation provided a number close to 2.5. This shows that simulation and experimentation are very close and taken the complexities of the problem in hand, the simulation proved to be more than accurate.

Figure 10. Pressure and Thrust Curves

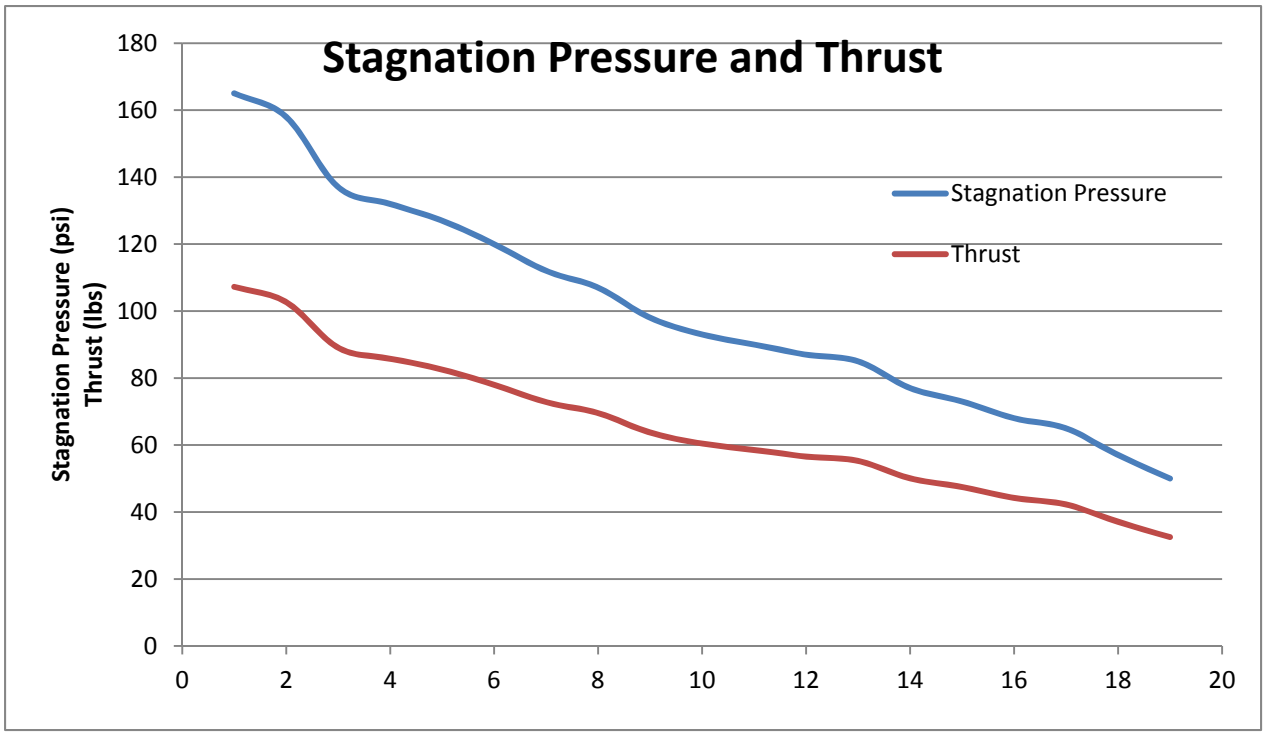

The following figure, is describing the relationship between the tank pressure and the thrust exerted at the piston heads. These data were obtained during the pitot tube experimentation. As it can be seen in this figure the thrust increases as the pressure at the inlet increases. This relationship was described and determined in the simulation process. The relationship seems to be almost linear. Even though the line in the graph is not completely straight, it can be assumed that the pressure at the inlet is related linearly to the thrust produced by the converging diverging nozzle. One reason that the line is not completely straight is because not all pressure regions were considered extensively. In order to cover most parts, the pressure regimes were divided in increments of 50 psi, with 50 psi being the starting pressure and 500 psi being the highest pressure.

In figure 12, the Mach number is plotted as a function of the inlet or also called tank pressure. In this graph the Mach number is shown to increase with increasing inlet pressure and reaches a high value of 2.67. Here the relationship also seems to be somewhat of a parapola. This is easily explained by looking back to figure 9 where the pressure ratio relationship is plotted. As mentioned earlier the Mach number is a function pressure ratio and thus the plots should be related as well. Another observation that can be made is that the Mach number will eventually decrease as the pressure foes below 100 psi. Even though there is a decrease, the flow remains supersonic.

Figure 11. Thrust vs. Inlet pressure

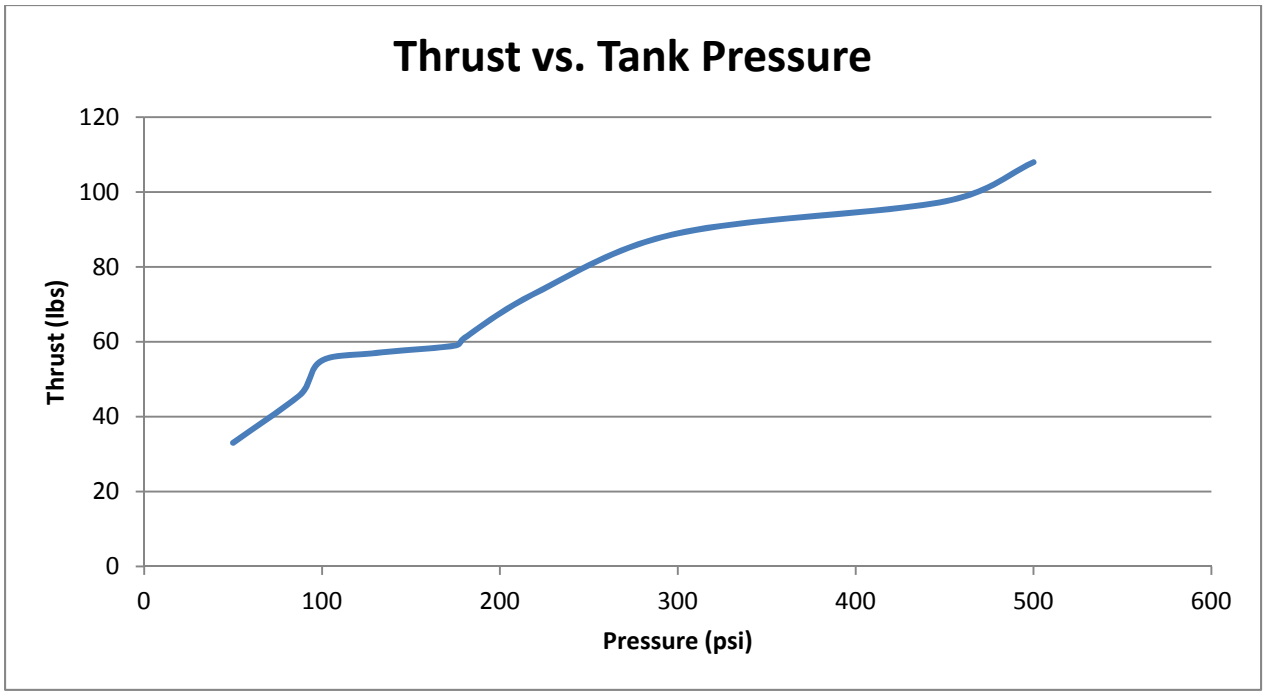

Figure 12. Mach vs. Inlet Pressure

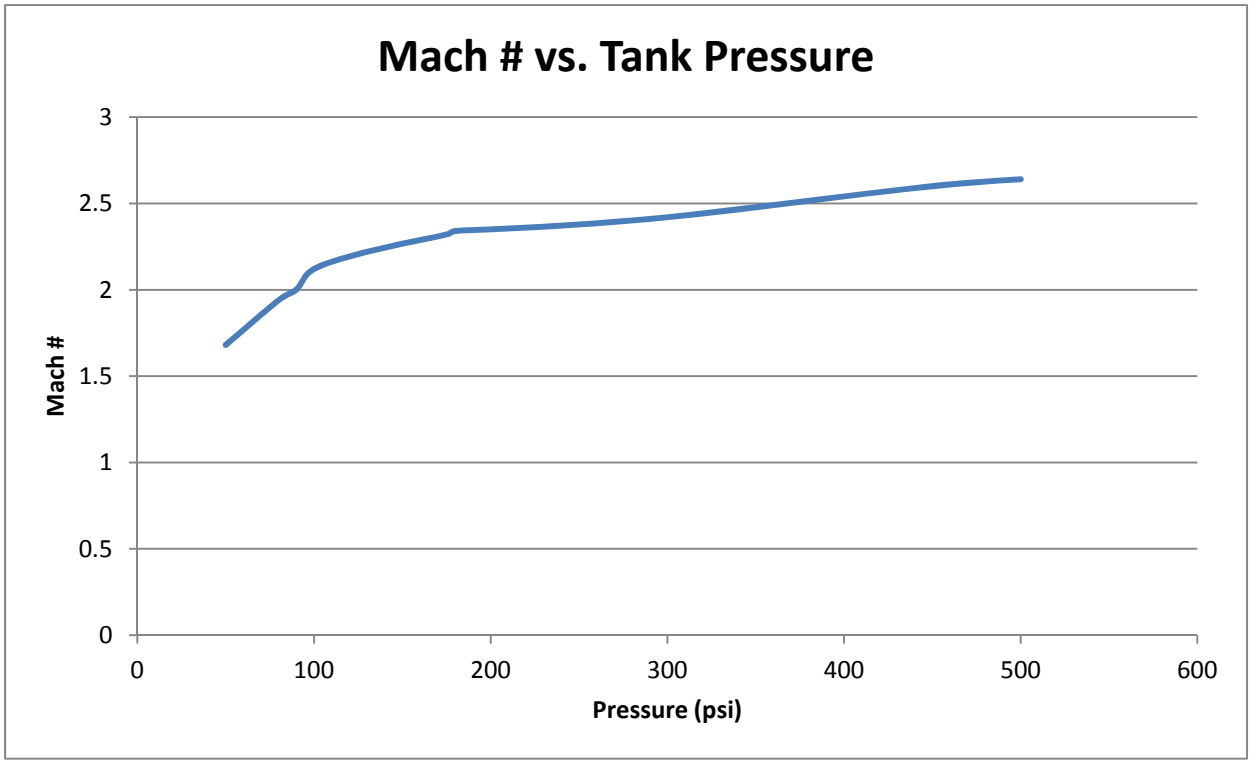

Table 2. Pitot Tube Experimentation Results

Tank Pressure (psi)	Stagnation	Static	Mach #	Thrust

500	165	8	2.64	107.25
450	150	8	2.6	97.5
300	136	9	2.42	88.4
220	112	8	2.36	72.8
180	93	7	2.34	60.45
175	90	7	2.32	58.5
130	87	8	2.22	56.55
100	84	9	2.12	54.6
90	72	9	2	46.8
80	65	9	1.94	42.25
50	50	10	1.68	32.5

The table above summarizes the results found with the pitot static tube experimentation. The figure below presents the stagnation and static pressure relationship for an inlet pressure of 50 psi. It is obvious that as the stagnation pressure increases rapidly, the static pressure decreases below atmospheric, which indicates the existence of supersonic flow.

Figure 13. Pitot Tube at 50 psi

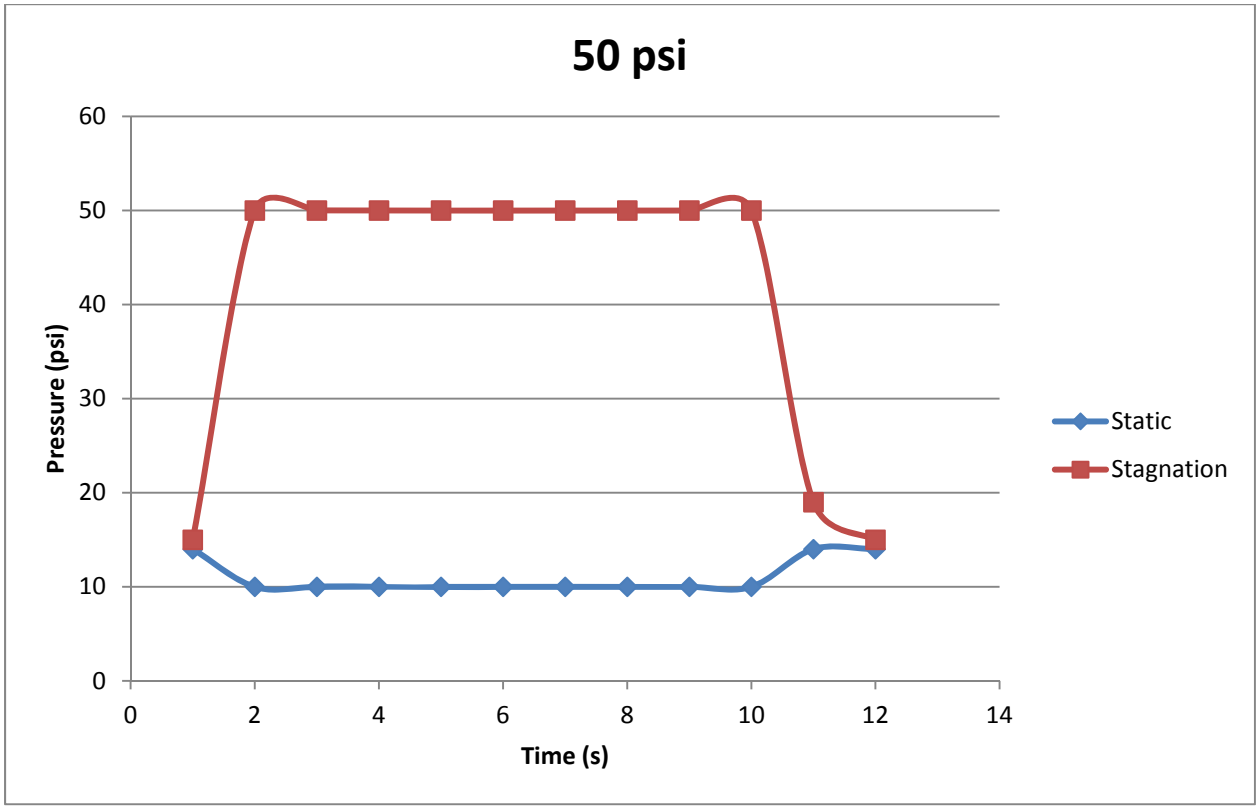

Figure 14. Pitot Tube at 300 psi

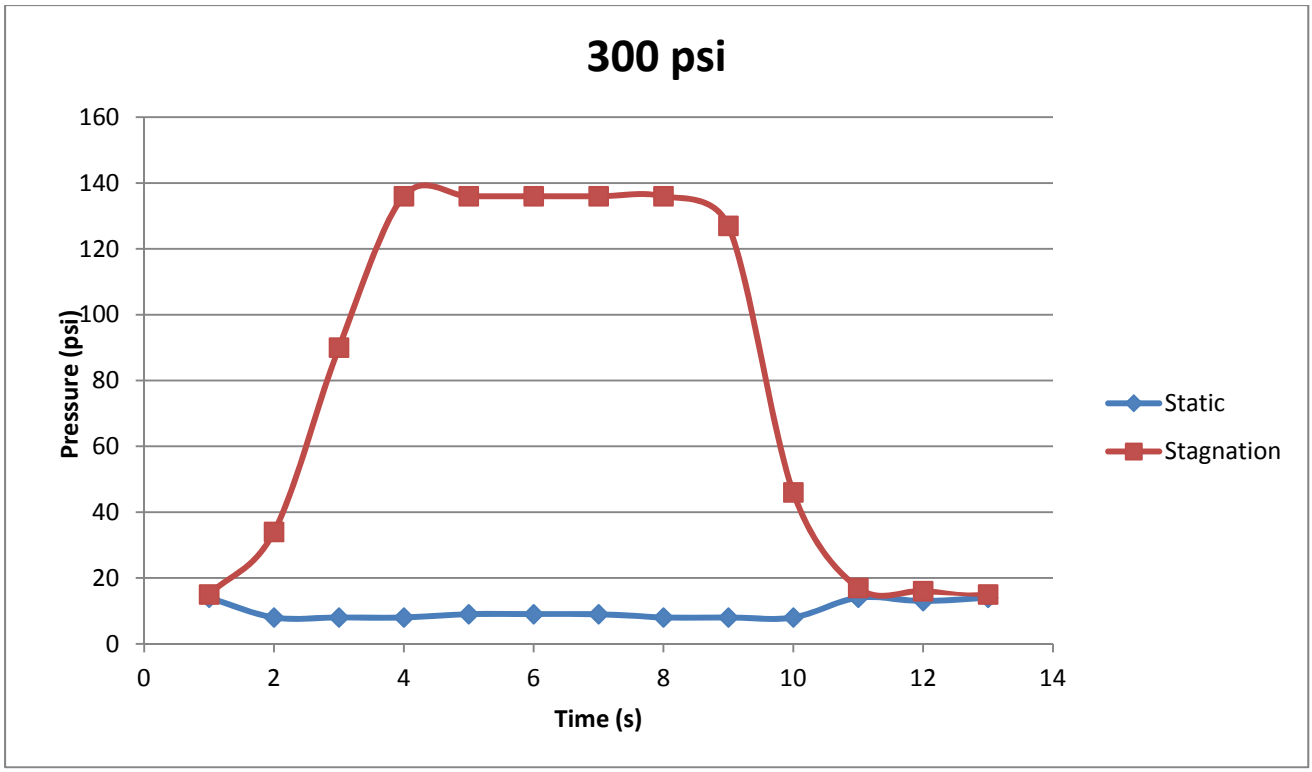

Both figures 14 and 15, present the relationship of the stagnation and static pressures for given inlet pressure conditions. In these figures, an interesting fact is that during the experimentation procedure, the response of the stagnation pressure transducer sensor became slower than at lower pressure regimes. For instance at 300 psi, the stagnation pressure reaches its maximum within 3 seconds, while for 50 psi, it reaches the maximum stagnation pressure within half a second. This shows that the flow is fully developed in a much slower pace in higher inlet pressures but at the same time reach much higher stagnation pressures.

This characteristic can be seen in the figure below. Figure 15 is basically describing the relationship of the stagnation and the static pressure at the exit of the converging diverging nozzle as experienced by the pitot static tube. In this case, the stagnation pressure reaches its maximum within 4 seconds and reaches a high value of 165 psi. This number results in a pressure ratio of 0.047 that yields a Mach number of 2.67.

As seen in all the pitot tube experiment plots, there is plenty of evidence that the designed converging diverging nozzle reaches supersonic velocities in the majority of the pressure regime that the air is stored at. The fact that the flow reaches supersonic speeds and the thrust produced at the exit of the converging diverging nozzle is high enough to move the piston heads of the engine, proves the point that the selection of such a nozzle is suitable for the third stage of CAES. As shown in table 2, the thrust values are in close agreement with the predicted values from the simulation process. This also proves that not only the converging diverging nozzle

design is the most appropriate one but also that the simulation is in complete agreements with the experimentation and the design process.

Figure 15. Pitot Tube at 500 psi

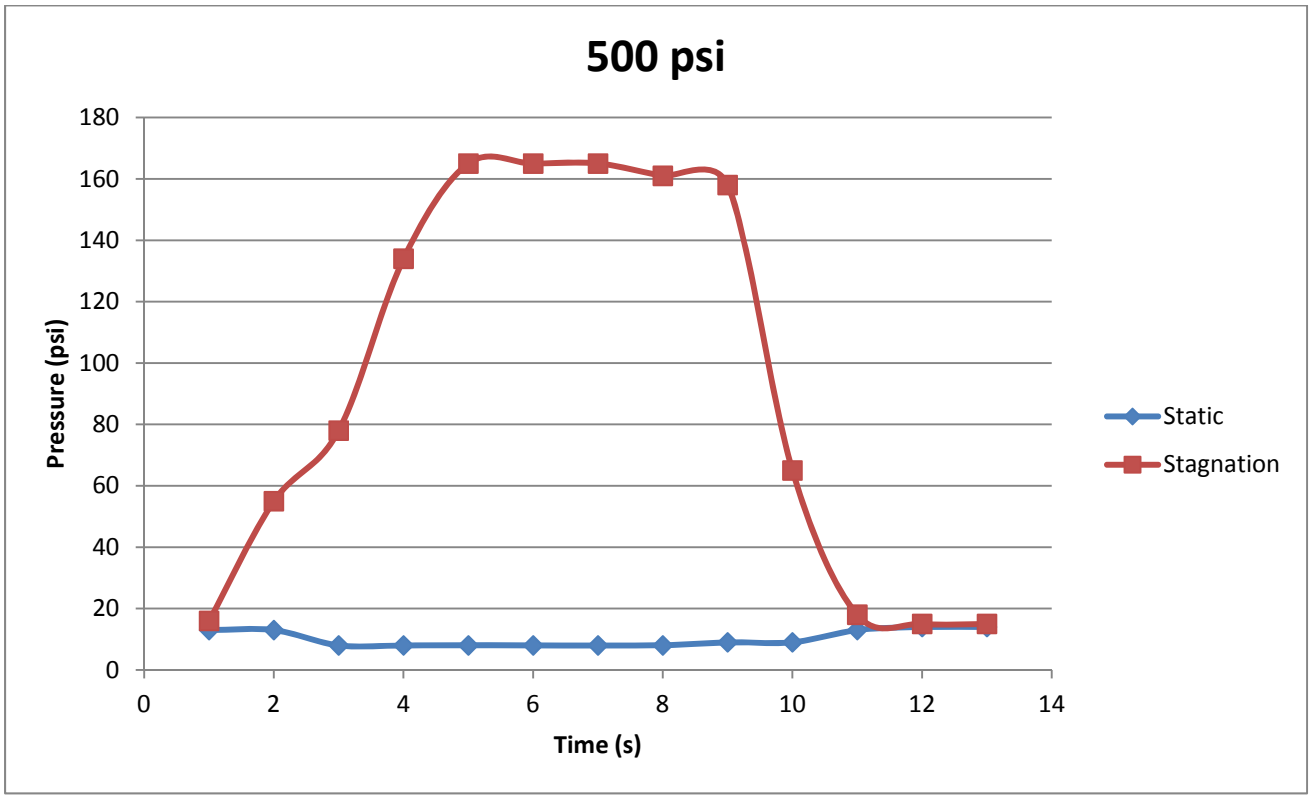

The LoadCell experiment was performed with different piping but was mainly tested with 1" piping diameter in the inlet of the converging diverging nozzle. The data were mainly collected to be compared to the pitot tube measurements. The LoadCell was placed on the exit of the converging diverging nozzle simulating the piston head moving boundary condition. The expected results in this experiment were the measurement of thrust with respect to time. The main objective of this experiment was to obtain more results in order to compare them to the experimental results of the pitot tube. Data acquisition was performed using the software that the LoadCell was integrated to. The platform on which the LoadCell was placed, played a significant role and it was made sure that the LoadCell was appropriately supported. Also the LoadCell placement was a major factor as being accurately placed on the exit of the CDN and at the same time it was made sure that the platform of the LoadCell didn't deflect due to the placement of the LoadCell.

The following figures show the measured values by the LoadCell for different inlet pressures. These plots and values were compared to the simulation and pitot probe experimentation. In figure 16 the highest thrust achieved is 43 lbs. In Figure 17 a higher inlet pressure is recorded which reaches around 87 lbs.

Figure 16

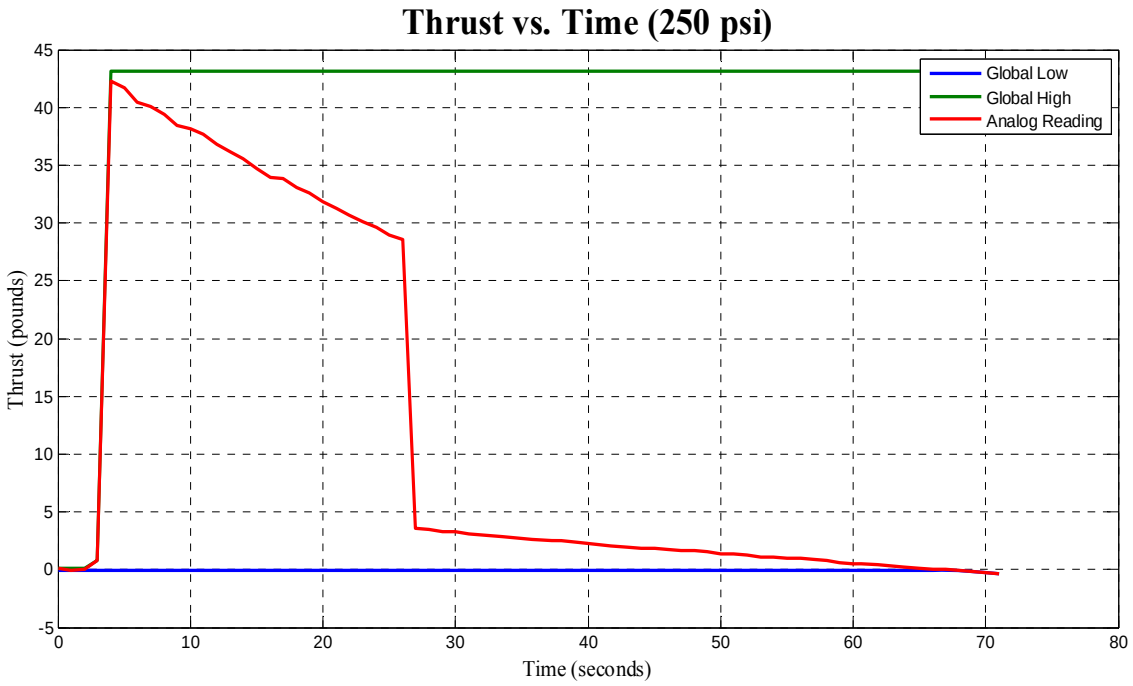

Figure 17

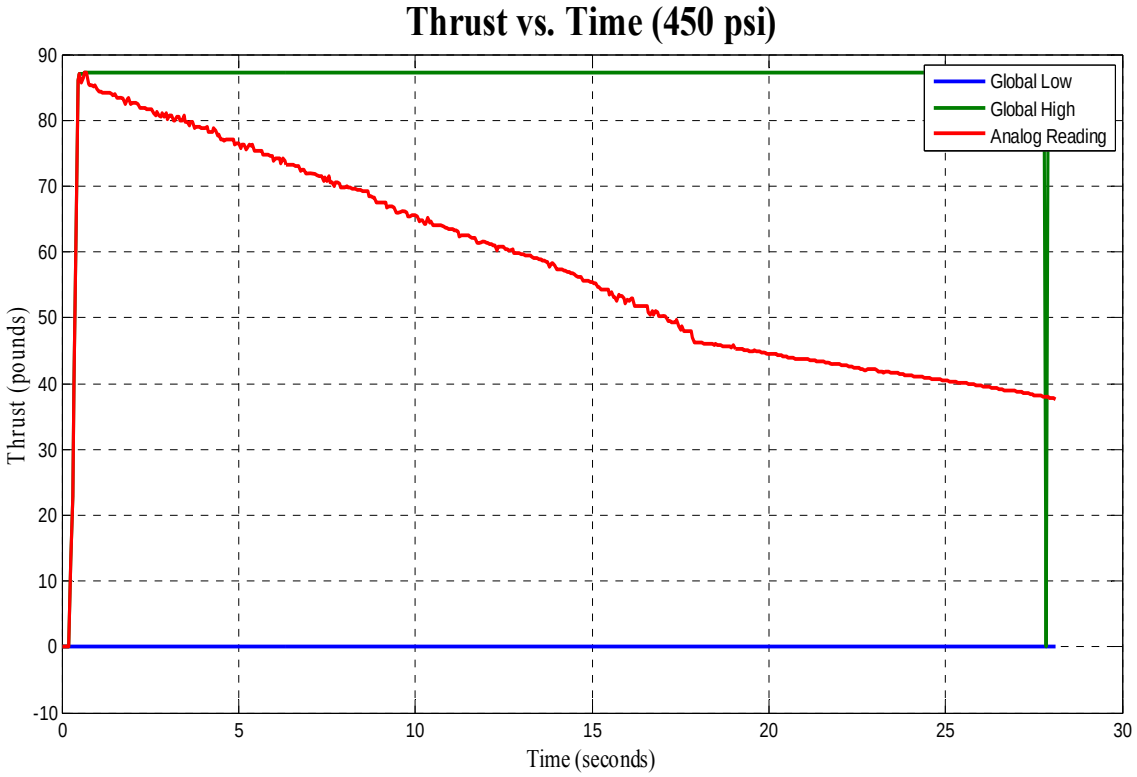

Figure 18

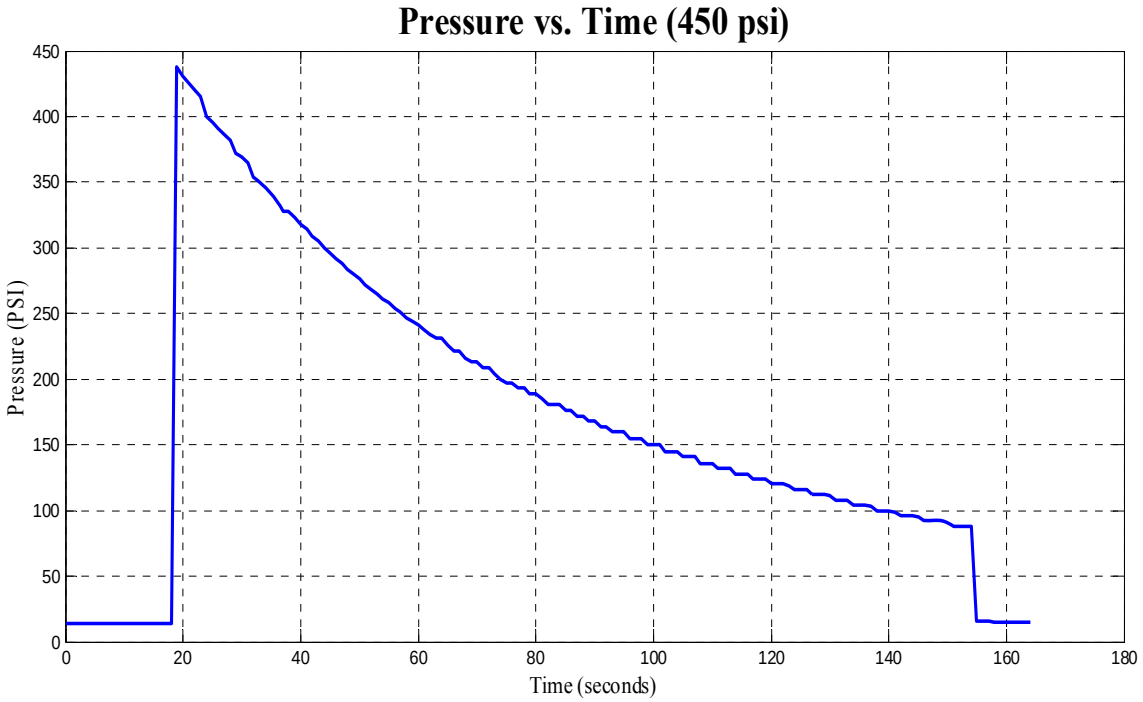

Figure 19

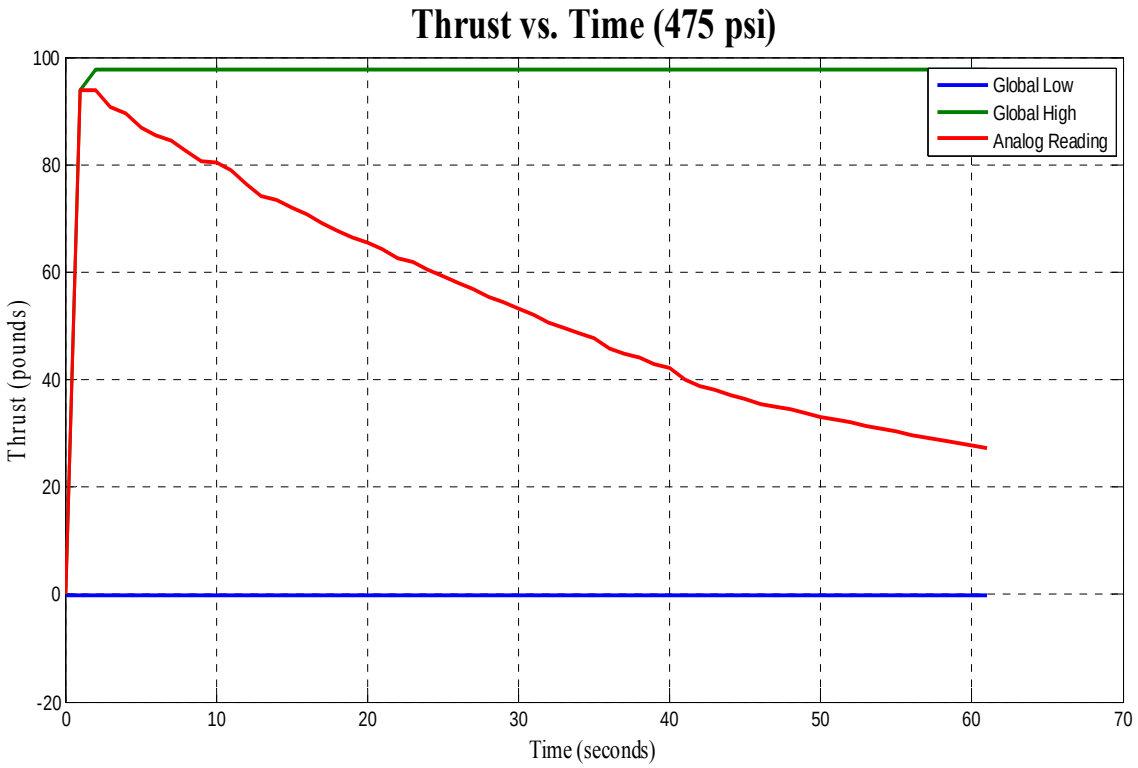

Figure 20

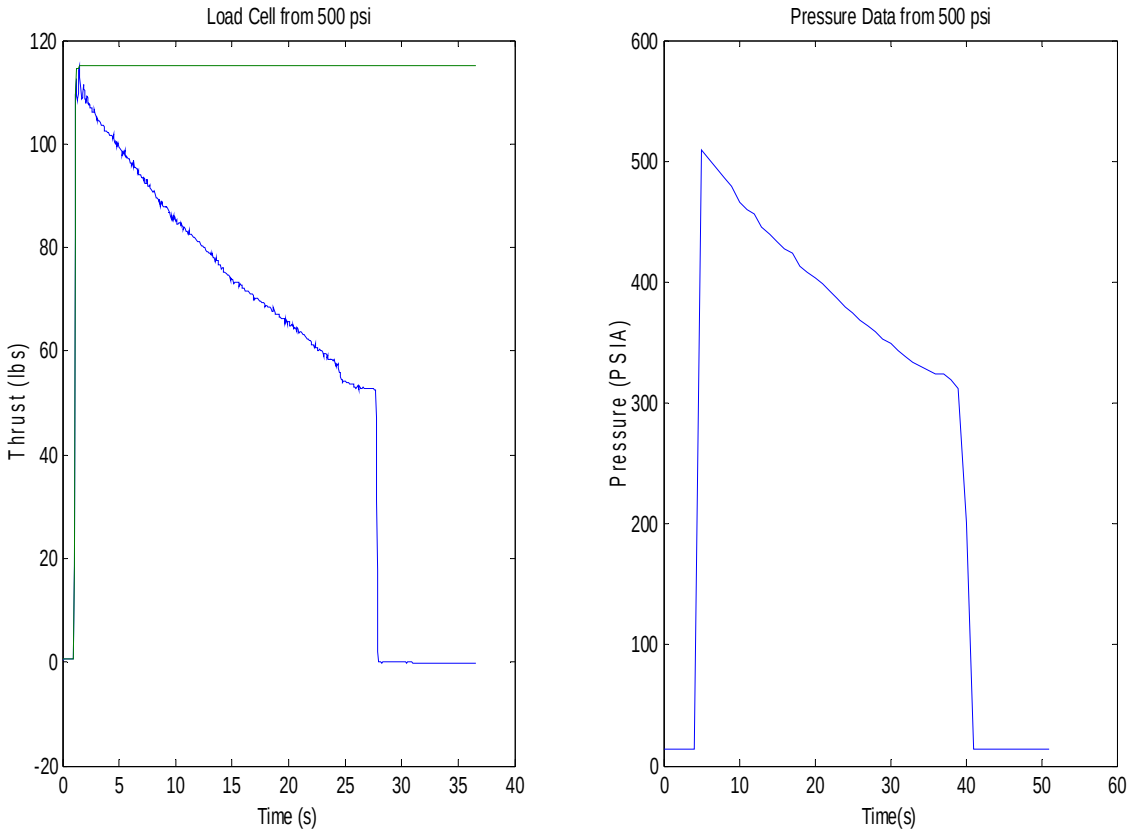

The figures above present the thrust and pressure curves as they were recorded during the LoadCell experimentation and they can easily be compared with the thrust curves produced during the simulation and pitot tube experimentation process. In particular, figure 18 shows the pressure drop that was recorded by an in line pressure transducer. This was done in order to determine whether the expectations, for a smooth pressure drop in the expansion process, would be realistic. In figure 20 it is quite obvious that the thrust and pressure drop curve are in agreement. There are no unexpected cut offs or abnormal decreases and the time frame for both the curves to reach their minimum is almost identical. In figure 19 the highest thrust recorded is 98 lbs, while in figure 20 the higher thrust recorded is 110 lbs. This is expected since the inlet pressure increases and as described through the simulation process, as the inlet pressure increases, the thrust output increases as well. This also proves that there were no inconsistencies in the experimentation process and all results were in agreement with the expectations that the simulation process provided. Another observation that can be made by looking at the above figures is that the thrust reaches its maximum value almost instantly and there are no indications of time delay. Therefore, the nozzle will be able to provide the maximum force on the piston head within half a second of the time that the air will be released at the inlet.

Figure 21

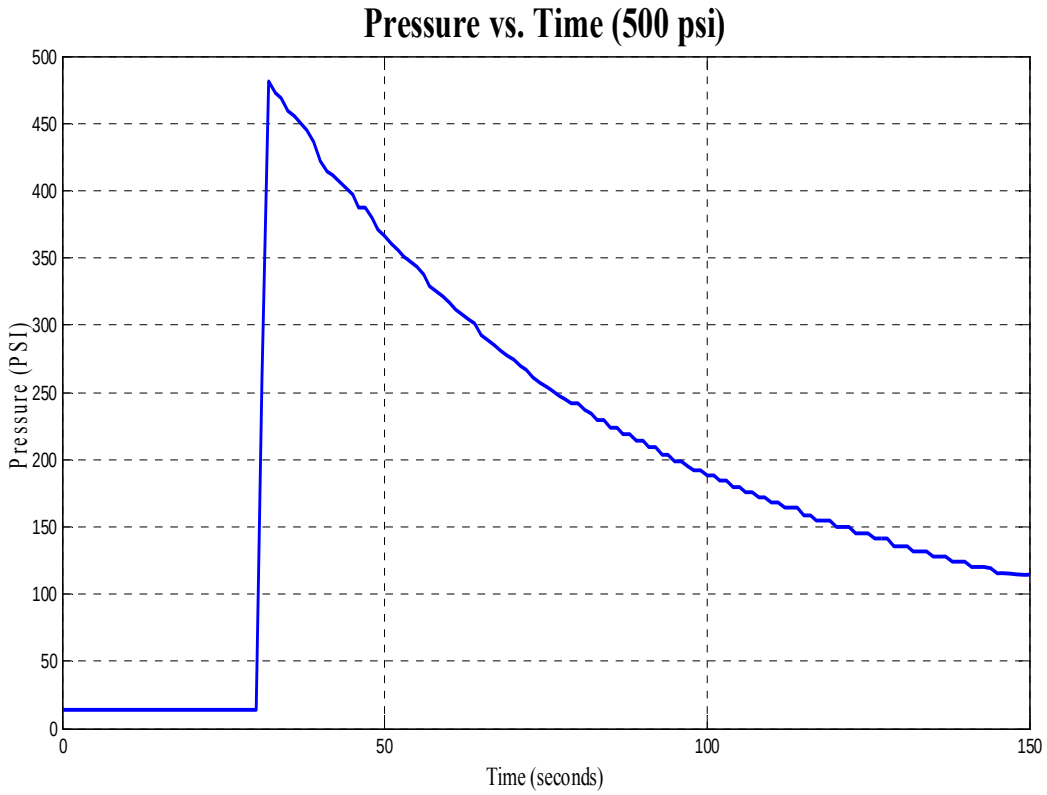

The figure above shows the pressure drop from a 500 psi inlet pressure. This was measured using a pressure transducer and it presents the predicted pressure drop curve experienced in the expansion stage of CAES.The table below outlines the line pressure and maximum thrust recorded in terms of inlet tank pressure. As seen, the highest number recorded in thrust is 110.7 lbs. Both simulation and pitot tube experimentation provided very close answers of 106.8 and 107 lbs respectively.

Table 3. LoadCell Experimentation Results

Tank Pressure (psi)	Line Pressure (psi)	Max Thrust (lb)
500	481	110.68
300	328	61.38
275	298	50.75
225	260	35.25
150	195	24.49

Figure 22. LoadCell Experimentation Results

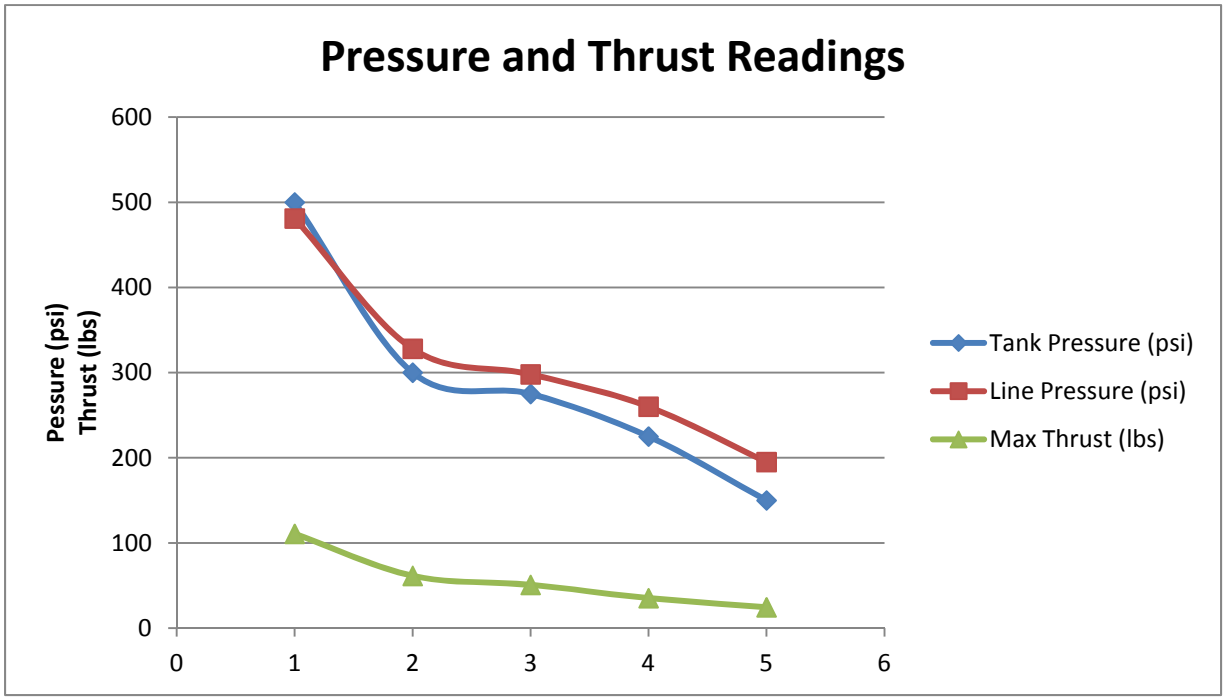

In conclusion, CFD analysis has proven that by increasing pressure, the current converging diverging nozzle design can produce the required thrust to operate the pneumatic motor. It has also been proven that this is done efficiently, since the converging diverging nozzle consumes the same amount of air as a normal cylinder head would, but at the same time it produces a much increased amount of thrust. An addition to the increased thrust that the converging diverging nozzle will deliver, increasing the inlet pressure will also increase the amount of thrust expected. This will obviously result into more kinetic energy produced by the camshaft and ultimately, a greater ability of producing electricity.

Comparing the simulation results to the experimentation data it is obvious that are in agreement. As seen, the highest number recorded for thrust in the LoadCell experiments is 110.7 lbs., while both simulation and pitot tube experimentation provided very close answers of 106.8 and 107 lbs respectively. In this way it is proven that the converging diverging nozzle design is the most appropriate element for expanding compressed stored air. The graphs of the stagnation and the thrust curve from the pitot tube experiments are in agreement with the numbers produced by the LoadCell experiments. Also the Mach number reached was 2.67 while the prediction in the simulation provided a number close to 2.5. Therefore, simulation and experimentation are very close. Considering the complexities of the flow analysis in the converging diverging nozzle, the simulation proved to be very accurate.

Method of Characteristics

In the course of designing various types of nozzles, the Method of Characteristics was used to create different types of contours and smoother profiles of converging diverging nozzles. A code of Method of Characteristics was used in MATLAB code that and there were three different types of nozzle contours and various flow characteristic curves that were produced using this code. Below are the three different cases. As it can be seen, the contour of the nozzle is different for each case and the flow characteristics vary as well.

Flow characteristics for a Mach 2.33 nozzle design

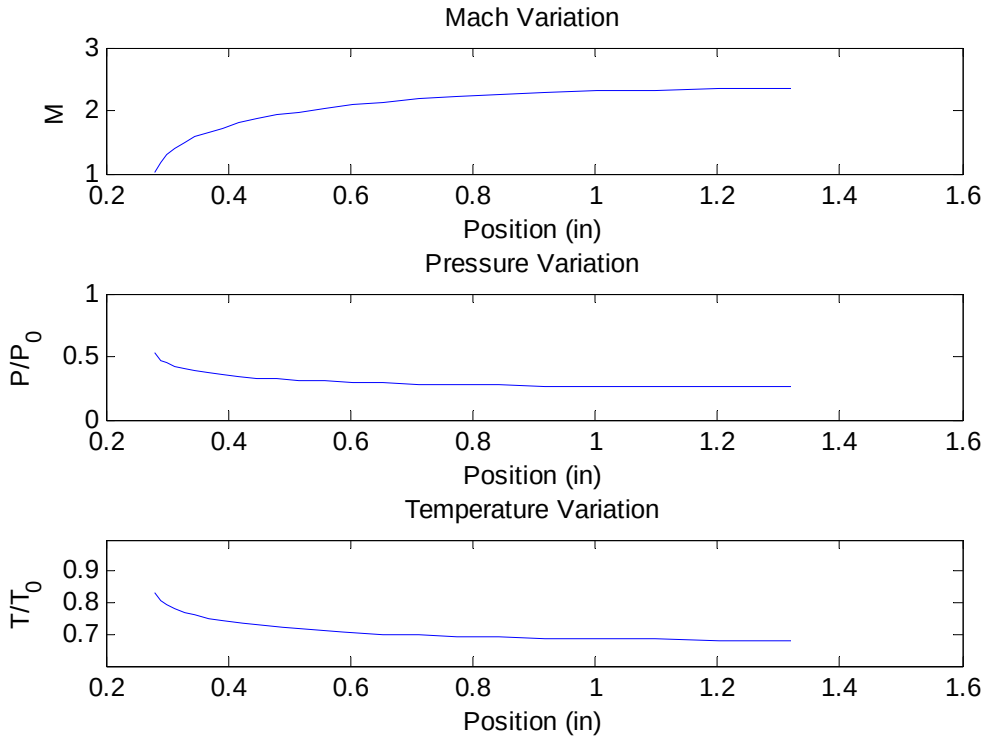

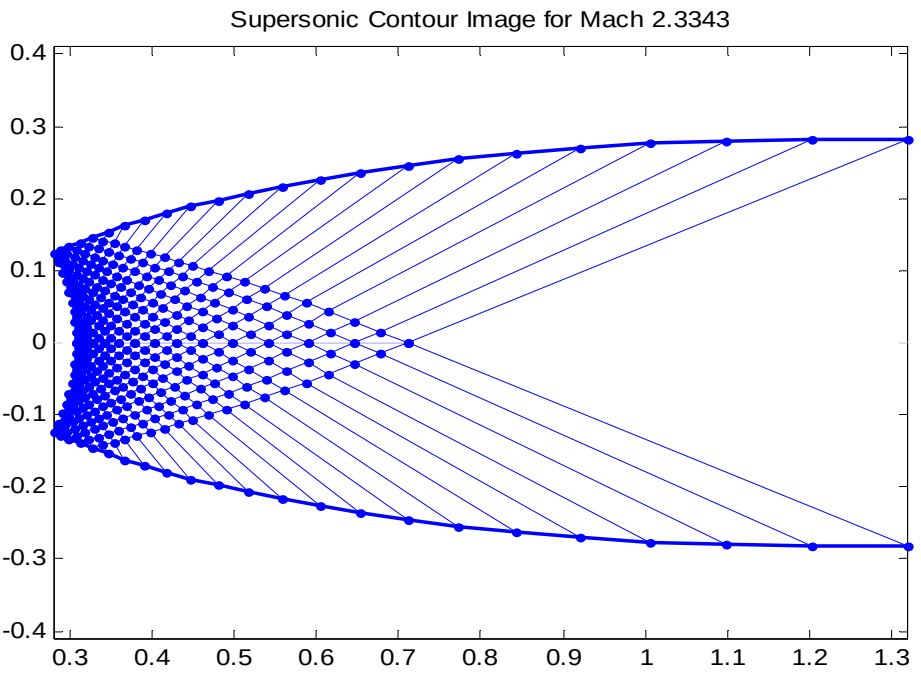

Flow characteristics for a Mach 3.68 nozzle design

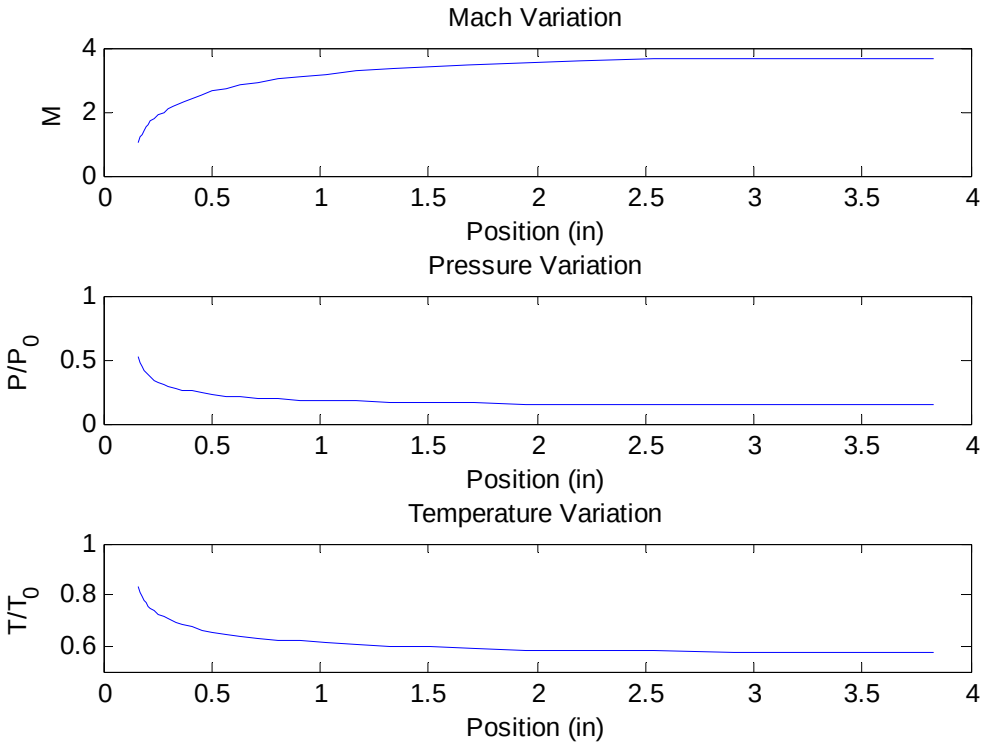

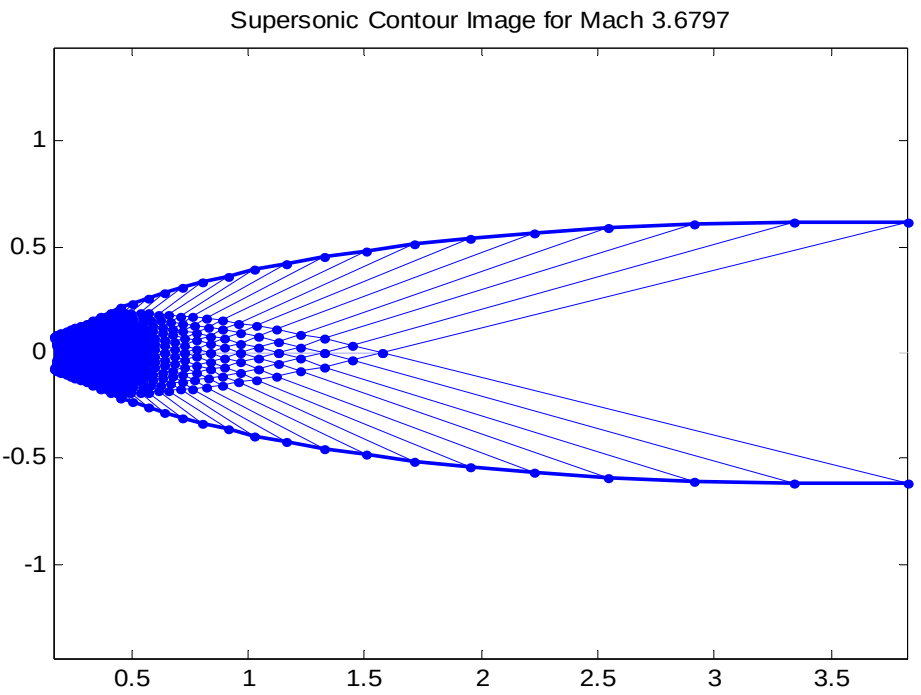

Flow characteristics for a Mach 3.99 nozzle design

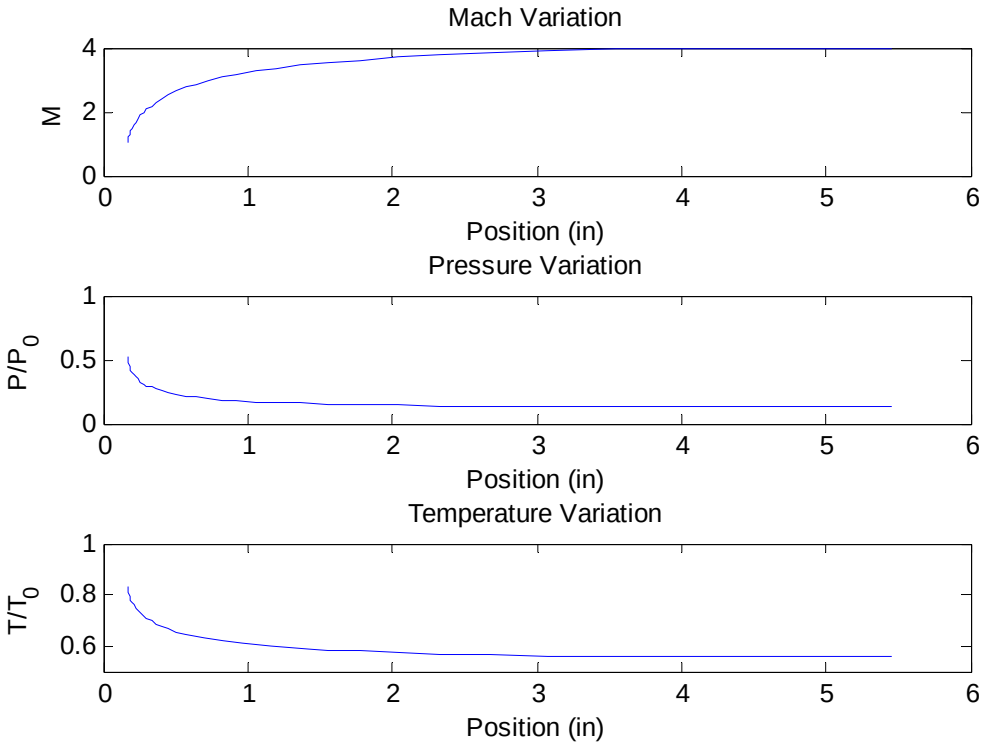

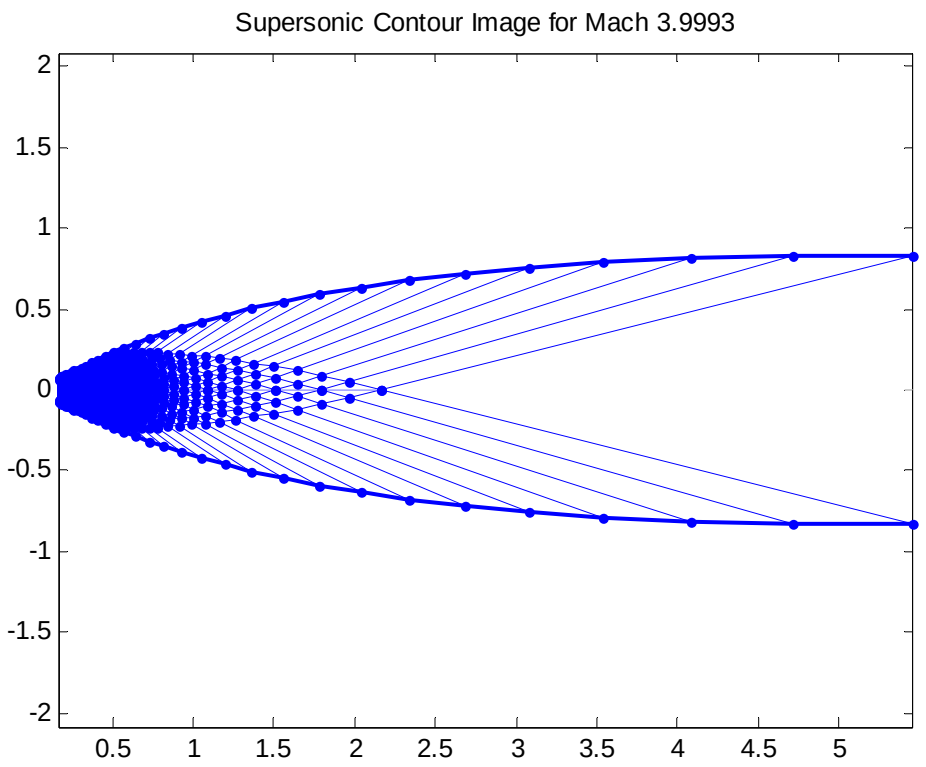

As it can be seen from the contour profiles for different Mach numbers, the diverging section of the CDN is different as the Mach number changes. This results in having a different pressure ratio, temperature and Mach number variation along the length of the nozzle.